However, amlodipine showed no such reduction compared with the 'no treatment' group (Fig. 4). In contrast, there were no significant differences in the lipid profiles, systolic blood pressure, and heart rates among the differently treated groups of mice (Online Table 2). There were also no significant differences in levels of multiple cytokines and chemokines among the groups (Online Table 3).

4. Discussion

The present study demonstrated that treatment with a newly developed CCB, azelnidipine, at 3 and 10 mg/kg attenuated the development of advanced atherosclerosis induced by balloon injury and hypercholesterolemia in non-human primates (cynomolgus monkeys).

To assess the clinical significance of our present finding, the dose range of azelnidipine is important. We recently reported that the C_{max} of azelnidipine at 3 and 10 mg/kg per day were 36 ± 17 and 107 ± 17 ng/mL, respectively, in cynomolgous monkeys [12]. The C_{max} after oral administration of 16 mg of azelnidipine to hypertensive subjects is reported to be 48 ± 19 ng/mL [10]. Therefore, it is reasonable to consider that in regards to plasma concentrations (C_{max}), the 3 mg/kg dose is within a clinically relevant dose range, and the 10 mg/kg dose is higher than the clinical dose range (i.e. is a pharmacological dose range) in monkeys. Furthermore, we also reported that the dose of azelnidipine used in the present study did not affect systemic arterial blood pressure and heart rate in cynomolgus monkeys under conscious conditions [12]. Therefore, it is suggested that the beneficial effects of azelnidipine on atherosclerosis as observed in monkeys were not due to its effects on serum lipids or arterial blood pressure (Table 1).

To examine the mechanisms underlying azelnidipine's anti-atherosclerotic effects, we examined a representative local oxidative stress marker with fluorescent dihydroethidium staining in monkeys. Our data clearly showed that azelnidipine at low and high doses nearly eliminated the increase in the fluorescence (i.e. the increase in oxidative stress) in neointima cells in atherosclerotic lesions. Similar potent anti-oxidant effects of azelnidipine were also reported by Jinno et al. [9], who showed that azelnidipine prevented the increases in fluorescent dihydroethidium signals and NAD(P)H oxidase activity in the neointima induced by cuff-induced vascular injury. Because the neointima usually consists of activated smooth muscle cells, the present data suggest that mediation of local oxidative stress in neointimal smooth muscle cells is one of the major pathways by which azelnidipine exerts its anti-atherosclerotic actions.

Table 1
Serum MCP-1 levels in cynomolgus monkeys

	Baseline (week 0)	24 weeks after treatment
Control	44 ± 5	$61 \pm 5^{*}$
Azelnidipine 3 mg/kg	46 ± 4	47 ± 5
Azelnidipine 10 mg/kg	47 ± 4	37 ± 4

Data are expressed as mean ± S.E.M. $n = 12$.
* $P < 0.05$ vs. baseline.

Because inflammatory and proliferative processes induced by oxidative stress play a central role in atherogenesis [15], we next used immunohistochemistry to examine the expression of MCP-1 and PDGF. We and others have demonstrated that increased monocyte-mediated inflammation is associated with greater neointimal formation after stenting [16,17] and that anti-MCP-1 gene therapy [18,19] or administration of blocking antibody against the MCP-1 receptor markedly reduces neointimal formation after vascular injury. In addition to inflammation, the proliferation of vascular smooth muscle cells induced by PDGF plays a crucial role in atherogenesis. Here, we found reduced MCP-1 and PDGF immunoreactivity in the neointimal smooth muscle cells after treatment with azelnidipine at 3 and 10 mg/kg. Normalization of serum MCP-1 levels was also noted with azelnidipine treatment. These data suggest that the anti-atherosclerotic effects of azelnidipine might be attributable to the inhibition of oxidative stress-induced upregulation of MCP-1 and PDGF in the neointimal cells.

However, immunohistochemical analysis of the cellular composition of the neointima showed that azelnidipine had no effect on macrophage infiltration. We therefore hypothesized that azelnidipine was having a direct effect on vascular smooth muscle cells. The date presented here from vascular smooth muscle cells in culture shows that azelnidipine significantly inhibits PDFG-induced proliferation and migration of vascular smooth muscle cells. In addition, this inhibitory effect was associated with decreased PDGF-induced production of MCP-1. We recently found that blocking MCP-1 partly inhibits PDGF-induced proliferation and migration of vascular smooth muscle cells in culture (author's unpublished data, 2006). In addition, it was recently reported that MCP-1 not only mediates monocyte-related inflammation, but also mediates transformation, proliferation, and migration of vascular smooth muscle cells [20]. Collectively, these data suggest that MCP-1 is involved in the mechanism of azelnidipine's inhibitory effects on PDGF-induced proliferation and migration of vascular smooth muscle cells.

To investigate whether the observed anti-atherosclerotic effects are unique to azelnidipine, we therefore compared effects of azelinidipine versus amlodipine in ApoE-KO mice. Azelnidipine at 10 mg/kg per day, but not amlodipine at 10 mg/kg per day, reduced atherosclerotic plaque size after 8 weeks of a high cholesterol diet. Neither azelnidipine nor amlodipine had any effect on hemodynamic parameters or on blood lipid profiles, indicating that the observed differential effects between the two drugs are independent of any effects on serum lipid levels or arterial blood pressure. Our present data are not contradictory to previous articles showing no definitive effects in atherosclerositic mice [21,22] or monkeys [23]. The mechanism underlying the differential

effects of these two CCBs is unclear, but may be related to azelnidipine's high lipid solubility/high vascular affinity [23]. Recently, Ma et al. reported that the inhibitory effect of azelnidipine on iNOS-catalyzed NO production from vascular smooth muscle cells in culture was greater than that of amlodipine or nifedipine [24]. Moreover, azelnidipine is reported to inhibit H_2O_2-induced production of 8-isoprostane from human arterial endothelial cells in culture to a greater extent than other same class CCBs (amlodipine and nifedipine) [25].

There are several caveats in interpreting the clinical significance of our present study. First, although we have shown anti-atherosclerotic effects of azelnidipine in non-human primates, the experimental and clinical evidence for the anti-atherosclerotic effects of CCBs remains controversial. Recent clinical trials with CCBs did not directly address the reduction of atherosclerosis and/or cardiovascular mortality in patients with atherosclerotic vascular disease [26]. Second, it deserves mentioning that the vast majority of patients with atherosclerotic vascular disease is not treated with CCB alone, but with combination of CCB plus statin, angiotensin receptor blockers and etc. [27]. In this regard, recent reports shows a synergistic effects of CCBs and statin etc. on progression of atherosclerosis. It is likely therefore that clinical benefits of CCBs on atherosclerosis might be overt in combination of other vasculoprotective drugs, such as statins.

In conclusion, this study presents experimental evidence that oral administration of azelnidipine at a clinically relevant dose and at a pharmacological dose attenuates advanced atherosclerosis in non-human primates. The beneficial effects were associated with reduced local oxidative stress, reduced MCP-1 and PDGF expression, and reduced smooth muscle cell proliferation/migration in the neointima. Notably, the anti-atherosclerotic effect seems to be unique to azelnidipine, rather than a class-effect of CCBs in respect to our data with ApoE-KO mice. These data in non-human primates suggest potential clinical benefits of azelnidipine might be beneficial as a "vasculoprotective CCB" in patients with atherosclerotic vascular disease. Further clinical trials are needed to prove this hypothesis.

Acknowledgements

This study was supported by Grants-in-Aid for Scientific Research (14657172, 14207036) from the Ministry of Education, Science, and Culture, Tokyo, Japan and by unlimited research grant from Sankyo Co., Tokyo, Japan.

Appendix A. Supplementary data

Supplementary data associated with this article can be found, in the online version, at doi:10.1016/j.atherosclerosis.2007.03.036.

References

[1] Pitt B, Byington RP, Furberg CD, et al. Effect of amlodipine on the progression of atherosclerosis and the occurrence of clinical events. PREVENT Invest Circ 2000;102:1503–10.
[2] Major outcomes in high-risk hypertensive patients randomized to angiotensin-converting enzyme inhibitor or calcium channel blocker vs. diuretic: the Antihypertensive and Lipid-Lowering Treatment to Prevent Heart Attack Trial (ALLHAT). JAMA 2002;288:2981–97.
[3] Julius S, Kjeldsen SE, Weber M, et al. Outcomes in hypertensive patients at high cardiovascular risk treated with regimens based on valsartan or amlodipine: the VALUE randomised trial. Lancet 2004;363:2022–31.
[4] Jorgensen B, Simonsen S, Endresen K, et al. Restenosis and clinical outcome in patients treated with amlodipine after angioplasty: results from the Coronary AngioPlasty Amlodipine REStenosis Study (CAPARES). J Am Coll Cardiol 2000;35:592–9.
[5] Nissen SE, Tuzcu EM, Libby P, et al. Effect of antihypertensive agents on cardiovascular events in patients with coronary disease and normal blood pressure: the CAMELOT study: a randomized controlled trial. JAMA 2004;292:2217–25.
[6] Poole-Wilson PA, Lubsen J, Kirwan BA, et al. Effect of long-acting nifedipine on mortality and cardiovascular morbidity in patients with stable angina requiring treatment (ACTION trial): randomised controlled trial. Lancet 2004;364:849–57.
[7] Mason RP, Marche P, Hintze TH. Novel vascular biology of third-generation L-type calcium channel antagonists: ancillary actions of amlodipine. Arterioscler Thromb Vasc Biol 2003;23:2155–63.
[8] Henry PD, Bentley KI. Suppression of atherogenesis in cholesterol-fed rabbit treated with nifedipine. J Clin Invest 1981;68:1366–9.
[9] Jinno T, Iwai M, Li Z, et al. Calcium channel blocker azelnidipine enhances vascular protective effects of AT1 receptor blocker olmesartan. Hypertension 2004;43:263–9.
[10] Kuramoto K, Ichikawa S, Hirai A, et al. Azelnidipine and amlodipine: a comparison of their pharmacokinetics and effects on ambulatory blood pressure. Hypertens Res 2003;26:201–8.
[11] Yagil Y, Lusting A, Azelnidipine. (CS-905), a novel dihydropyridine calcium channel blocker with gradual onset and prolonged duration of action. Cardiovasc Drugs Rev 1995;13:137–48.
[12] Nakano K, Egashira K, Tada H, et al. A third-generation, long-acting, dihydropyridine calcium antagonist, azelnidipine, attenuates stent-associated neointimal formation in non-human primates. J Hypertens 2006;24:1881–9.
[13] Kitamoto S, Nakano K, Hirouchi Y, et al. Cholesterol-lowering independent regression and stabilization of atherosclerotic lesions by pravastatin and by antimonocyte chemoattractant protein-1 therapy in nonhuman primates. Arterioscler Thromb Vasc Biol 2004;24:1522–8.
[14] Inoue S, Egashira K, Ni W, et al. Anti-monocyte chemoattractant protein-1 gene therapy limits progression and destabilization of established atherosclerosis in apolipoprotein E-knockout mice. Circulation 2002;106:2700–6.
[15] Egashira K. Clinical importance of endothelial function in arteriosclerosis and ischemic heart disease. Circ J 2002;66:529–33.
[16] Farb A, Weber DK, Kolodgie FD, Burke AP, Virmani R. Morphological predictors of restenosis after coronary stenting in humans. Circulation 2002;105:2974–80.
[17] Welt FG, Rogers C. Inflammation and restenosis in the stent era. Arterioscler Thromb Vasc Biol 2002;22:1769–76.
[18] Egashira K, Zhao Q, Kataoka C, et al. Importance of monocyte chemoattractant protein-1 pathway in neointimal hyperplasia after periarterial injury in mice and monkeys. Circ Res 2002;90:1167–72.
[19] Egashira K. Molecular mechanisms mediating inflammation in vascular disease: special reference to monocyte chemoattractant protein-1. Hypertension 2003;41:834–41.
[20] Denger S, Jahn L, Wende P, et al. Expression of monocyte chemoattractant protein-1 cDNA in vascular smooth muscle cells: induction

of the synthetic phenotype: a possible clue to SMC differentiation in the process of atherogenesis. Atherosclerosis 1999;144:15–23.

[21] van de Poll SW, Delsing DJ, Jukema JW, et al. Raman spectroscopic investigation of atorvastatin, amlodipine, and both on atherosclerotic plaque development in APOE*3 Leiden transgenic mice. Atherosclerosis 2002;164:65–71.

[22] Candido R, Allen TJ, Lassila M, et al. Irbesartan but not amlodipine suppresses diabetes-associated atherosclerosis. Circulation 2004;109:1536–42.

[23] Takai S, Kim S, Sakonjo H, Miyazaki M. Mechanisms of angiotensin II type 1 receptor blocker for anti-atherosclerotic effect in monkeys fed a high-cholesterol diet. J Hypertens 2003;21:361–9.

[24] Ma J, Kishida S, Wang GQ, et al. Comparative effects of azelnidipine and other Ca2+-channel blockers on the induction of inducible nitric oxide synthase in vascular smooth muscle cells. J Cardiovasc Pharmacol 2006;47:314–21.

[25] Shinomiya K, Mizushige K, Fukunaga M, et al. Antioxidant effect of a new calcium antagonist, azelnidipine, in cultured human arterial endothelial cells. J Int Med Res 2004;32:170–5.

[26] Lichtlen PR, Hugenholtz PG, Rafflenbeul W, et al. Retardation of angiographic progression of coronary artery disease by nifedipine. Results of the International Nifedipine Trial on Antiatherosclerotic Therapy (INTACT). INTACT Group investigators. Lancet 1990;335:1109–13.

[27] Jukema JW, Zwinderman AH, van Boven AJ, et al. Evidence for a synergistic effect of calcium channel blockers with lipid-lowering therapy in retarding progression of coronary atherosclerosis in symptomatic patients with normal to moderately raised cholesterol levels. The REGRESS Study Group. Arterioscler Thromb Vasc Biol 1996;16:425–30.

ELSEVIER

Atherosclerosis 194 (2007) 309–316

ATHEROSCLEROSIS

www.elsevier.com/locate/atherosclerosis

Catheter-based adenovirus-mediated anti-monocyte chemoattractant gene therapy attenuates in-stent neointima formation in cynomolgus monkeys

Kaku Nakano, Kensuke Egashira*, Kisho Ohtani, Gang Zhao, Kota Funakoshi, Yoshiko Ihara, Kenji Sunagawa

Department of Cardiovascular Medicine, Graduate School of Medical Sciences, Kyushu University, 3-1-1, Maidashi, Higashi-ku, Fukuoka, Japan

Received 29 June 2006; received in revised form 27 September 2006; accepted 18 October 2006
Available online 28 November 2006

Abstract

We have previously demonstrated great benefit from anti-monocyte chemoattractant protein-1 (MCP-1) gene therapy by "systemic" transfer of an N-terminal deletion mutant of human MCP-1 (called 7ND) gene into skeletal muscle for treatment of restenosis and atherosclerosis. However, recent evidence suggests that "local" gene transfer may be a clinically relevant approach. We therefore tested the hypothesis that catheter-based adenovirus-mediated anti-MCP-1 gene therapy attenuates stent-associated neointima formation.

Bare metal stents were implanted in iliac arteries of cynomolgus monkeys fed a high cholesterol diet. Immediately after the stenting procedure, normal saline or recombinant adenoviral vector containing LacZ or the 7ND gene was administered locally into the stenting site through a Remedy channel-delivery catheter. Compared to saline infusion or LacZ gene transfer, 7ND gene transfer markedly reduced inflammatory changes at an early stage and attenuated neointima formation after 4 weeks. This strategy also reduced the increased production of pro-inflammatory and growth-promoting factors such platelet-derived growth factor. No systemic adverse effects of 7ND gene transfer were detected. There were no significant differences in serum cholesterol levels among the three groups.

These data suggest that catheter-based adenovirus-mediated anti-MCP-1 gene therapy may be a clinically relevant and feasible strategy for treatment of in-stent restenosis.

Keywords: Restenosis; Inflammation; Monocyte; Gene therapy; Catheter intervention

1. Introduction

There is ample clinical and experimental evidence suggesting that inflammation plays a central role in the pathogenesis of restenosis [1–3]. Recruitment and activation of monocyte/macrophages are a major histopathologic finding after arterial injury. Because monocyte chemoattractant protein-1 (MCP-1) is a potent and specific chemokine for monocytes [3–5], an anti-inflammatory strategy targeting MCP-1 and its receptor (CCR2) may be an appropriate and reasonable approach for restenosis. We have previously devised a new strategy for anti-MCP-1 gene therapy, in which plasmid cDNA encoding a mutant MCP-1 gene is transfected into skeletal muscle [6]. This mutant MCP-1, called 7ND, lacks N-terminal amino acids 2–8 and has been shown to work as a dominant-negative inhibitor of MCP-1. This systemic approach (intramuscular transfection of the gene) is useful, because direct gene transfer into the injured arterial wall is not necessary, and roles of MCP-1 can be investigated under pathophysiological conditions *in vivo*. With this strategy, we have demonstrated that blocking MCP-1 signals reduces neointima formation after balloon- and stent-induced injury [7–10] and atherosclerosis [11,12] in animals, including non-human primates. Roque et al. [13] reported that CCR2-deficient mice display reduced neointimal hyperpla-

* Corresponding author. Tel.: +81 92 642 5358; fax: +81 92 642 5375.
E-mail address: egashira@cardiol.med.kyushu-u.ac.jp (K. Egashira).

0021-9150/$ – see front matter © 2006 Elsevier Ireland Ltd. All rights reserved.
doi:10.1016/j.atherosclerosis.2006.10.029

sia after intraluminal arterial injury. Horvath et al. [14] have demonstrated that blockade of the MCP-1 receptor (CCR2) with anti-CCR2 antibody reduced neointimal hyperplasia by 40% after stenting, by inhibiting monocyte infiltration in monkeys.

It is becoming accepted that, rather than a systemic approach, a local delivery strategy should be a reasonable anti-restenotic therapy with minimal systemic adverse effects [15]. Indeed, the development of drug-eluting stents (DES) has had a major impact on in-stent restenosis. Their safety and extreme effectiveness have been proven in a majority of lesions, after more than a million DES implantations. However, currently marketed first-generation DES use sirolimus or taxol as the drug that elicits nonspecific anti-proliferative effects, not only on vascular smooth muscle cells, but also other cell types such as endothelial cells. It is suggested that impaired endothelial function and regeneration lead to acceleration of restenosis and atherosclerosis, and to cardiovascular events [16]. Thus, the first-generation DES still have a number of limitations that include significant restenosis rates in certain high-risk patients or lesions (bifurcation lesions, small vessels, diabetes, etc.), delayed healing (excessive late inflammation, proliferation, and fibrin deposition), and a small number of cases of late in-stent thrombosis [15,17–19]. In addition, it should be noted that 30–40% of coronary atherosclerotic lesions may not be appropriate for stenting, due to small arteries or branch sites. Therefore, catheter-based local gene transfer of relevant genes may represent a clinically relevant and alternative approach for treatment of restenosis beyond the first-generation DES strategy.

Accordingly, this study was designed to investigate whether blockade of MCP-1 by catheter-based adenovirus-mediated local 7ND gene transfer is effective in attenuating stent-associated neointima formation in non-human primates. To gain clinical significance for the results, we used a non-human primate model of stent-associated neointima formation [7]. The Remedy channel-delivery catheter was used for local delivery, because it is adopted for human use, and thus relevant to the human interventional setting.

2. Methods

2.1. Adenoviral constructs

Human 7ND cDNA was constructed by recombinant polymerase chain reaction (PCR) using a wild-type human MCP-1 cDNA (Dr. T. Yoshimura, National Cancer Institute) as a template, and inserted into the BamH1 (5′) and Not1 (3′) sites of the pcDNA3 (Invitrogen) expression vector plasmid [6]. Twenty four nucleotides encoding FLAG epitope (DYKDDDDK) were added directly at the 3′ terminus of MCP-1 sequence. Adenovirus vectors encoding the 7ND gene (Ade-7ND) or galactosidase gene (Ade-LacZ) were generated by use of the Adenovirus Expression Vector Kit (Takara) according to the manufacturer's instructions.

2.2. Stent implantation and arterial gene transfer

The study protocol was reviewed and approved by the Committee on Ethics on Animal Experiments, Kyushu University Faculty of Medicine, and the experiments were conducted according to the Guidelines of the American Physiologic Society. A part of this study was performed at the Kyushu University Station for Collaborative Research.

Five-year-old adult male cynomolgus monkeys weighing 4–5 kg were fed laboratory diet containing 0.5% cholesterol, starting 2 months before stent implantation. Monkeys were anesthetized with ketamine hydrochloride (10 mg/kg IM) and sodium pentobarbital (30 mg/kg IV to effect), and underwent placement of a 3 mm × 15 mm stent in the external iliac artery, as described previously [20]. Immediately after stent implantation, the animals were randomly allocated to the normal saline, Ade-LacZ, or Ade-7ND group. Saline or adenovirus solution at amount of 2 mL (1.0×10^9 pfu) was locally infused through the Remedy channel balloon catheter (Boston Scientific Inc.) [21]. The titer of adenovirus used in this study was below the inflammatory threshold (1.6×10^9 pfu/body), as reported [22]. The Remedy is a triple-lumen local delivery device, and consists of a noncompliant angioplasty balloon surrounded by a set of 18–24 perforated channels (30 μm holes) [23]. These channels are directly connected to a separate infusion lumen, allowing independent low-pressure drug delivery. The balloon was inflated at 2 atm support pressure, and infusion of saline or virus solution was performed at 2 atm over 2 min. Efficient and relatively safe percutaneous gene transfer can reportedly be achieved without overt systemic toxicity using this approach [23], which is adopted for human use.

All monkeys were killed with a lethal dose of anesthesia 7 or 28 days after stenting for immunohistochemical and morphometric analysis. All animals received aspirin 81 mg/day and ticlopidine 100 mg/day until euthanasia.

2.3. Morphometric and immunohistochemical analysis

Stented arterial sections were excised and fixed for 24 h with 95% ethanol and 1% acetic acid. Each segment was divided into two parts at the center of the stent as described [20]. The proximal part was embedded in methyl methacrylate mixed with *n*-butyl methacrylate to allow for sectioning through metal stent struts. Serial sections were stained with elastica van Gieson and hematoxylin-eosin (HE). To evaluate the in-stent neointima formation, areas of internal elastic lamina, lumen, media, and neointima were measured.

The distal part was used for immunohistochemical analysis. After stent struts were gently removed with micro forceps, the tissue was dehydrated, embedded in paraffin, and cut into

5-μm thick slices. They were subjected to immunostaining using antibodies against macrophage/monocytes (HAM56, Dako), endothelial cells (CD31, Dako), PDGF-B (Mochida), IL-1β (Endogen), CCR2 (Sigma), or with non-immune mouse IgG (Zymed). Following avidin–biotin amplification, the slides were incubated with diaminobenzidine and counterstained with hematoxylin.

Morphometric analysis was performed by the use of a microscope with a computerized digital image-analysis system by a single observer who was blind to the treatment protocol.

2.4. Blood cholesterol measurements

Plasma total cholesterol levels were determined with commercially available kits (Wako Pure Chemicals).

2.5. Biochemical measurements

Plasma concentrations of human IL-8, TGF-β, and oxidized LDL were measured using an ELISA kit (R & D). To detect MCP-1 transgene expression indirectly, tissue concentrations of human MCP-1 were also measured by the use of an ELISA kit (R & D). Although we avoided using high titers of adenovirus that may cause inflammatory reactions [22], adenovirus vectors may cause virus-related adverse effects or toxicity. To examine potential systemic adverse effects, relevant biochemical markers were measured.

2.6. Efficiency of adventitial gene transfer

The efficiency of arterial gene transfer was determined in monkeys and rabbits. In monkeys, the expression of FLAG protein in stented arteries after 7days of stenting were evaluated by western blot analysis, as described previously [6]. In brief, the same amount of extracted protein (25 μg for each experiment) was loaded for SDS-PAGE/immunoblot analysis using anti-FLAG M2 monoclonal antibodies (Sigma). The regions containing MCP-1 proteins were visualized by LAS-1000 (Fujifilm).

We also determined the expression of 7ND in rabbits, as we reported previously [21]. Male Japanese white rabbits weighing 3.0–3.5 kg were anesthetized and underwent stent placement, and LacZ gene transfer was performed as described above. The transfection efficiency was measured 4 days after LacZ transfection by X-gal staining of sections from the target artery and calculated as follows: 100× (X-gal positive cells/total number of cells in a section).

2.7. Statistical analysis

Data are expressed as the mean ± S.E. Statistical analysis of differences was compared by ANOVA and Bonferroni's multiple comparison tests. A level of $P < 0.05$ was considered statistically significant.

3. Results

3.1. Inhibitory effects of Ade-7ND gene transfer on inflammatory and proliferative changes

Inflammatory (HAM56-positive monocyte/macrophage) and proliferative (PCNA-positive monocytes and medial smooth muscle cells) changes became evident 7 days after stenting in the stented arterial wall (Fig. 1). The 7ND gene transfer reduced these inflammatory and proliferating changes (Fig. 1).

3.2. Inhibitory effects of 7ND gene transfer on neointima formation

As we previously reported [7], in-stent neointima formation was evident 28 days after stenting. Quantitative analysis demonstrated a significant reduction of neointima formation and % stenosis in the Ade-7ND group compared with the saline and Ade-LacZ groups (Fig. 2). In contrast, there were no significant differences in area of internal elastic lamina among the three groups (Fig. 2).

Endothelial cell linings, monitored by CD31 immunoreactivity, were observed equally in the three groups (online Table 1). There was no significant treatment effect on serum cholesterol levels and body weight among the groups (online Tables 2 and 3).

3.3. Inhibitory effects of 7ND gene transfer on tissue expression of pro-inflammatory factors

Immunohistochemical staining performed 7 days after stenting revealed increased immunoreactive PDGF-B, VEGF, and CCR2 in cells in the neointima, smooth muscle cells in the media, and in cells in the adventitia in the saline and Ade-LacZ groups. These changes were reduced in the Ade-7ND group (Fig. 3A).

We also measured serum concentrations of IL-8, TGF-β, and oxLDL 7 days after stenting. 7ND gene transfer partially but significantly reduced the increase in serum IL-8 and oxLDL concentrations. 7ND gene transfer did not affect the increase in serum TGF-β levels (Fig. 3B).

3.4. No adverse effects of 7ND gene transfer

White blood cell counts, inflammatory markers, and biochemical markers were measured (online Table 3). These data show no systemic adverse effects of 7ND gene transfer.

3.5. Serum and tissue concentrations of MCP-1 plus 7ND

We could not find an MCP-1 ELISA kit that differentiated between human and monkey MCP-1. Thus, this "human MCP-1" ELISA kit detects both 7ND and native monkey MCP-1. The tissue concentration of MCP-1 plus

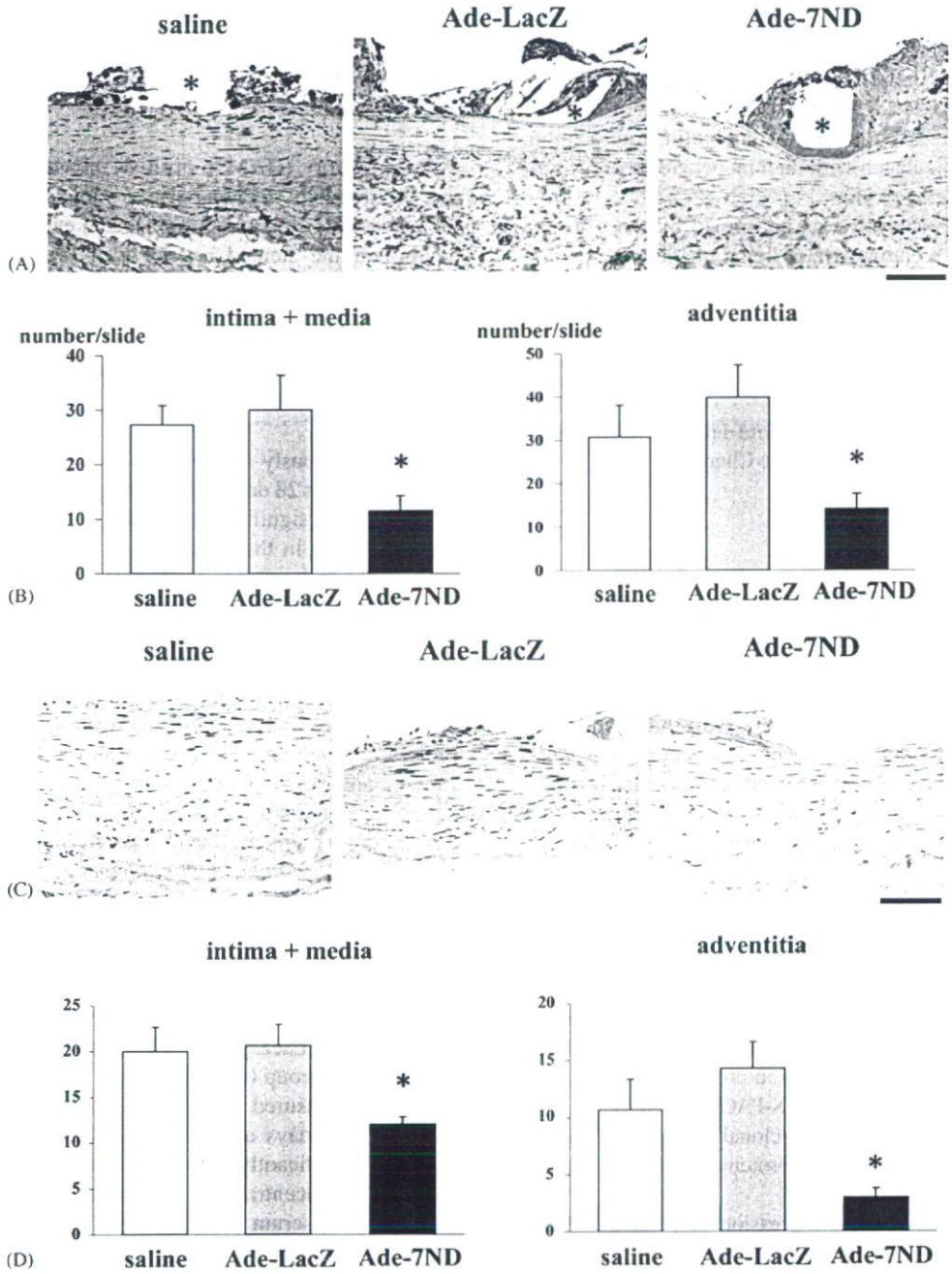

Fig. 1. Inhibitory effects of 7ND gene transfer on local inflammation and proliferation. (A) Effect of the 7ND gene transfer on local inflammation (HAM56-positive monocyte/macrophages) 7 days after stenting. Asterisk (*) indicates stent strut sites. Bar = 100 μm. (B) Summary of quantitative analysis ($n = 7$ each). Positive cell counts per section in the intima plus media (left) and in the adventitia (right) are shown. $^{*}P < 0.01$ vs. the saline or Ade-LacZ group. (C) Effect of the 7ND gene transfer on local proliferation (PCNA-positive monocytes and medial smooth muscle cells) 7 days after stenting. (D) Summary of quantitative analysis ($n = 7$ each). Positive cell counts per section in the intima plus media (left) and in the adventitia (right) are shown. $^{*}P < 0.01$ vs. the saline or de-LacZ group.

7ND at 7 days after stenting was higher in stented artery sites from the saline (120 ± 42 pg/mg protein) and Ade-LacZ (132 ± 46 pg/mg protein) groups than in unstented normal artery (24 ± 12 pg/mg protein), indicating increased production of MCP-1 from stented artery sites. Because, there was no significant difference in values between the saline and Ade-LacZ groups, we suggest that transfer of the LacZ gene did not affect the degree of MCP-1 production. Importantly, the tissue MCP-1 + 7ND levels were 2- to 3-fold higher in the stented artery sites from the Ade-7ND group

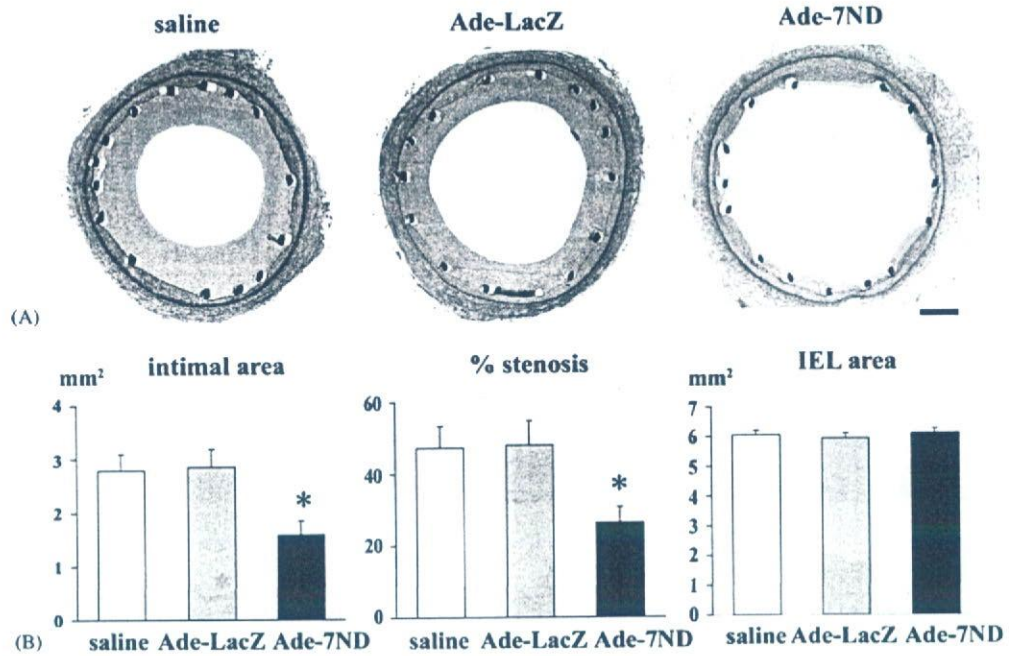

Fig. 2. Inhibitory effect of 7ND gene transfer on in-stent neointimal formation. (A) Iliac artery sections from the saline, the Ade-LacZ, and the Ade-7ND group 28 days after stenting, stained with elastic van Gieson. Bar = 500 μm. (B) Effect of 7ND gene transfer on intimal area, % stenosis, and IEL area 28 days after stenting ($n = 7$ each). $^{*}P < 0.01$ vs. the saline groups.

(564 ± 128 pg/mg protein) than in those from the saline and Ade-LacZ groups, indicating possible production of 7ND from the transfected arterial sites as the result of transgene expression.

3.6. Transgene expression in monkeys and rabbits

In monkeys, western blot analysis for FLAG protein showed that FLAG/7ND protein was produced in stented arteries (online Figure I). We further examined, 4 days after stent implantation and gene transfection in the rabbit iliac artery, the expression of β-galactosidase was noted at the Ade-LacZ-transfected site (Fig. 4). Nuclear staining for LacZ was localized mostly in the intima and the lumenal side of the media, and to a lesser extent in the adventitia. As reported by other investigators [23,24], the transfection efficiency was 9.2 ± 0.6% ($n = 4$).

4. Discussion

This study reports, for the first time, that blockade of MCP-1 by catheter-based adenovirus-mediated local gene transfer of 7ND markedly reduced in-stent neointima formation in non-human primates (cynomolgus monkeys). Transgene expression was confirmed directly by FLAG/7ND protein expression after Ade-7ND transfer and X-gal staining of stenting sites after Ade-LacZ transfer, and indirectly by measuring arterial tissue concentrations of MCP-1 plus 7ND after Ade-7ND transfer. Another important point is that the magnitudes of inhibitory effects on in-stent neointima formation afforded by this local gene transfer strategy (neointimal area in control and Ade-7ND groups: 2.8 ± 0.3 mm² and 1.4 ± 0.2 mm², respectively) are greater than those afforded by "systemic" gene transfer strategy in our previous study [7] (neointimal areas in control and 7ND gene transfer groups: 3.2 ± 0.2 mm² and 2.4 ± 0.2 mm², respectively). No non-specific inflammatory effects on in-stent neointima were detected in the Ade-LacZ group. Furthermore, our findings in non-human primates may have clinical significance, because many therapeutic strategies that have proven effective in reducing restenosis in nonprimate animal models have failed to demonstrate substantial effect on human restenosis. Although it is uncertain which animal model is most appropriate for the evaluation of in-stent restenosis, non-human primate models may have advantages over nonprimate animal models, because, (1) vascular inflammatory and proliferative responses to injury in non-human primates are presumed to be closer to those in humans than other, non-primate models and (2) the results of safety tests can be applied to humans. Therefore, the use of non-human primates may allow us to evaluate the efficacy and safety of therapies such as 7ND gene transfer on in-stent neointimal formation in more reliable conditions. These findings suggest that catheter-based adenovirus-mediated gene transfer of 7ND is a feasible approach for treatment of restenosis, with minimal potential systemic adverse effects.

It is well known that inflammatory changes (monocyte recruitment and activation) induced by stent-induced injury are critical in the pathogenesis of in-stent restenosis

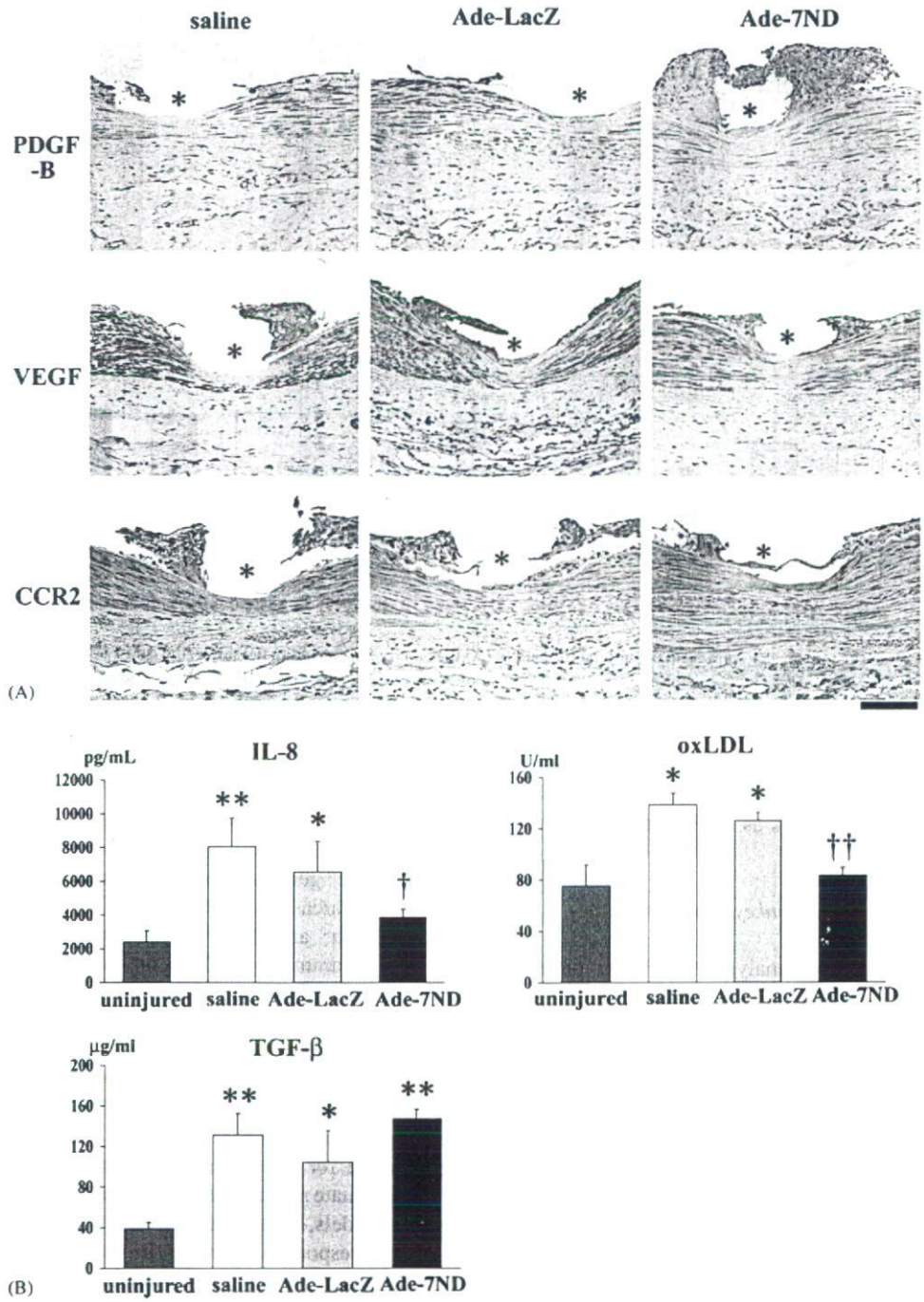

Fig. 3. Effects of 7ND gene transfer on immunohistochemical expression of PDGF-B, VEGF, and CCR2 and on plasma concentrations of IL-8, oxLDL, and TGF-β. (A) Iliac artery sections from uninjured normal arteries, and those from the Ade-LacZ and Ade-7ND groups 7 days after stenting. They are stained immunohistochemically for PDGF-B, VEGF, and CCR2. Asterisk (*) indicates stent strut sites. Bar = 100 μm. (B) Plasma concentrations of IL-8, oxLDL, and TGF-β 7 days after stenting $^{*}P<0.05$, $^{**}P<0.01$ vs. uninjured normal control, $^{\dagger}P<0.05$, $^{\dagger\dagger}P<0.01$, vs. the saline group.

[3,25,26]. We and others have reported that (1) increased monocyte-mediated inflammation correlates positively with in-stent neointima formation [1,2] and (2) blockade of MCP-1 reduces neointima formation after vascular injury [7–10,13,14]. Because, we demonstrated here that catheter-based Ade-7ND transfer reduced inflammation, the beneficial effects of Ade-7ND transfer can be attributed to inhibition of MCP-1-mediated inflammation. It is also possible that Ade-7ND transfer reduced in-stent neointima formation by inhibiting the proliferation of vascular smooth muscle

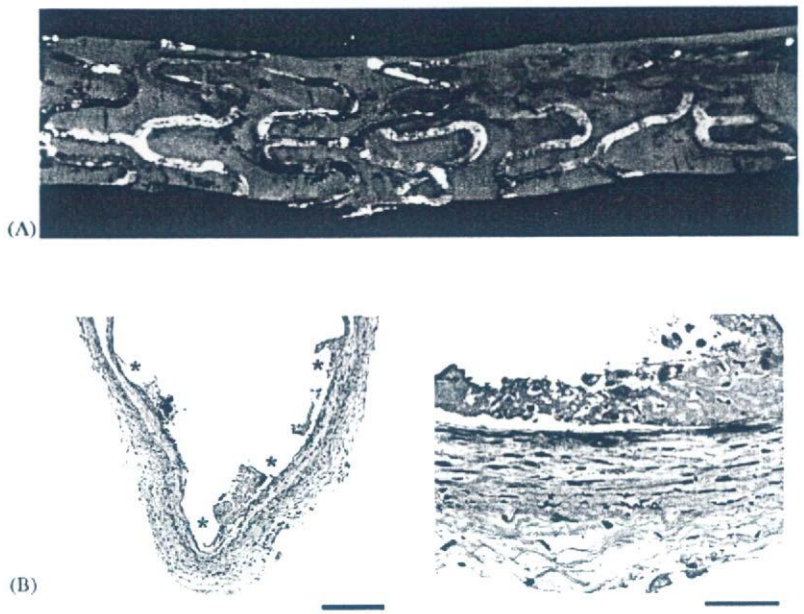

Fig. 4. Gene transfer into rabbit iliac stented artery after local infusion of de-LacZ via the Remedy delivery catheter. (A) Macroscopic picture of lumenal surface of the stented iliac artery staining with X-gal 4 days after transfection. Stented arterial segments were excised, cult longitudinally, and stained with X-gal. (B) X-gal-stained arterial cross-sections at low (right) and high (left) power of magnification. Asterisk (*) indicates stent strut sites. The bars indicate 400 μm (left) and 50 μm (right).

cells. Recent evidence suggests that vascular smooth muscle cells have a functional MCP-1 receptor (CCR2) [27]. In this study, local 7ND gene transfer attenuated (1) the appearance of proliferating smooth muscle cells and (2) the increased expression of mitogens of vascular smooth muscle cells (PDGF, VEGF, oxLDL) after stenting. Interestingly, local 7ND transfer reduced increased expression of CCR2 and IL-8, suggesting the presence of a positive-feedback loop to enhance inflammation and proliferation once vascular response to injury began. Therefore, it is possible that local 7ND gene transfer might reduce in-stent neointima formation by inhibiting inflammation, proliferation of vascular smooth muscle cells, or both.

In contrast, 7ND gene transfer did not affect endothelial regeneration, suggesting that the 7ND gene transfer may not impair the healing process of endothelial cells in stented arterial wall. This point may be an advantage of our approach over currently marketed first-generation DES. The Cypher (sirolimus) and Taxus (paclitaxel) stents impair regeneration of endothelial cells after stenting [28], and this may lead to impaired healing of the stented arterial wall. Hence, we presume that specific blockade of MCP-1-mediated signals in monocytes and smooth muscle cells, as described here using catheter-based local transfer of the 7ND gene, may provide a promising therapeutic strategy for restenosis with low potential toxicity.

In regard to clinical applicability, the potential systemic toxicity of catheter based adenovirus-mediated gene transfer deserves discussion. We demonstrated here that catheter-based adenovirus-mediated 7ND gene transfer induced no detectable inflammatory or immune reactions. We have previously reported that intramuscular systemic transfer of plasmid cDNA encoding the 7ND gene is nontoxic and safe in non-human primates [8,10,29], rabbits [7], rats [10], and mice [8]. In addition, mice lacking MCP-1 or CCR2 display no serious health problems. Furthermore, several protocols for adenovirus-mediated gene therapy have been in clinical trials, which reported no systemic adverse effects when the clinical trial protocol was performed properly. Overall, these toxicity data support the notion that this mode of gene therapy can be applied to human patients.

In conclusion, these data suggest that catheter-based adenovirus-mediated anti-MCP-1 gene therapy may be a clinically relevant and feasible therapeutic strategy for treatment of in-stent restenosis. If this mode of treatment is proven to be effective and safe, it could be used as an independent therapy for high-risk lesions, small vessels, or recurrent restenosis resistant to currently marketed DES. It could also be used as an alternative therapy beyond the first-generation DES strategy.

Acknowledgments

This study was supported by Grants-in-Aid for Scientific Research (14657172, 14207036) from the Ministry of Education, Science, and Culture, Tokyo, Japan; by Health Science Research Grants (Comprehensive Research on Aging and Health, and Research on Translational Research) from the Ministry of Health Labor and Welfare, Tokyo, Japan; by the

Program for Promotion of Fundamental Studies in Health Sciences of the Organization for Pharmaceutical Safety and Research, Tokyo, Japan.

Appendix A. Supplementary data

Supplementary data associated with this article can be found, in the online version, at doi:10.1016/j.atherosclerosis.2006.10.029.

References

[1] Farb A, Weber DK, Kolodgie FD, Burke AP, Virmani R. Morphological predictors of restenosis after coronary stenting in humans. Circulation 2002;105:2974–80.
[2] Welt FG, Rogers C. Inflammation and restenosis in the stent era. Arterioscler Thromb Vasc Biol 2002;22:1769–76.
[3] Egashira K. Molecular mechanisms mediating inflammation in vascular disease: special reference to monocyte chemoattractant protein-1. Hypertension 2003;41:834–41.
[4] Gerard C, Rollins BJ. Chemokines and disease. Nat Immunol 2001;2:108–15.
[5] Mukaida N, Harada A, Matsushima K. Interleukin-8 (IL-8) and monocyte chemotactic and activating factor (MCAF/MCP-1), chemokines essentially involved in inflammatory and immune reactions. Cytokine Growth Factor Rev 1998;9:9–23.
[6] Egashira K, Koyanagi M, Kitamoto S, et al. Anti-monocyte chemoattractant protein-1 gene therapy inhibits vascular remodeling in rats: blockade of MCP-1 activity after intramuscular transfer of a mutant gene inhibits vascular remodeling induced by chronic blockade of NO systhesis. FASEB J 2000;14:1974–8.
[7] Ohtani K, Usui M, Nakano K, et al. Antimonocyte chemoattractant protein-1 gene therapy reduces experimental in-stent restenosis in hypercholesterolemic rabbits and monkeys. Gene Ther 2004;11:1273–82.
[8] Egashira K, Zhao Q, Kataoka C, et al. Importance of monocyte chemoattractant protein-1 pathway in neointimal hyperplasia after periarterial injury in mice and monkeys. Circ Res 2002;90:1167–72.
[9] Mori E, Komori K, Yamaoka T, et al. Essential role of monocyte chemoattractant protein-1 in development of restenotic changes (neointimal hyperplasia and constrictive remodeling) after balloon angioplasty in hypercholesterolemic rabbits. Circulation 2002;105:2905–10.
[10] Usui M, Egashira K, Ohtani K, et al. Anti-monocyte chemoattractant protein-1 gene therapy inhibits restenotic changes (neointimal hyperplasia) after balloon injury in rats and monkeys. FASEB J 2002;16:1838–40.
[11] Ni W, Egashira K, Kitamoto S, et al. New anti-monocyte chemoattractant protein-1 gene therapy attenuates atherosclerosis in apolipoprotein E-knockout mice. Circulation 2001;103:2096–101.
[12] Inoue S, Egashira K, Ni W, et al. Anti-monocyte chemoattractant protein-1 gene therapy limits progression and destabilization of established atherosclerosis in apolipoprotein E-knockout mice. Circulation 2002;106:2700–6.
[13] Roque M, Kim WJ, Gazdoin M, et al. CCR2 deficiency decreases intimal hyperplasia after arterial injury. Arterioscler Thromb Vasc Biol 2002;22:554–9.
[14] Horvath C, Welt FG, Nedelman M, Rao P, Rogers C. Targeting CCR2 or CD18 inhibits experimental in-stent restenosis in primates: inhibitory potential depends on type of injury and leukocytes targeted. Circ Res 2002;90:488–94.
[15] Costa MA, Simon DI. Molecular basis of restenosis and drug-eluting stents. Circulation 2005;111:2257–73.
[16] Schmidt-Lucke C, Rossig L, Fichtlscherer S, et al. Reduced number of circulating endothelial progenitor cells predicts future cardiovascular events: proof of concept for the clinical importance of endogenous vascular repair. Circulation 2005;111:2981–7.
[17] Virmani R, Farb A, Guagliumi G, Kolodgie FD. Drug-eluting stents: caution and concerns for long-term outcome. Coron Artery Dis 2004;15:313–8.
[18] Virmani R, Guagliumi G, Farb A, et al. Localized hypersensitivity and late coronary thrombosis secondary to a sirolimus-eluting stent: should we be cautious? Circulation 2004;109:701–5.
[19] McFadden EP, Stabile E, Regar E, et al. Late thrombosis in drug-eluting coronary stents after discontinuation of antiplatelet therapy. Lancet 2004;364:1519–21.
[20] Hiasa K, Ishibashi M, Ohtani K, et al. Gene transfer of stromal cell-derived factor-1alpha enhances ischemic vasculogenesis and angiogenesis via vascular endothelial growth factor/endothelial nitric oxide synthase-related pathway: next-generation chemokine therapy for therapeutic neovascularization. Circulation 2004;109:2454–61.
[21] Ohtani K, Egashira K, Hiasa K, et al. Blockade of vascular endothelial growth factor suppresses experimental restenosis after intraluminal injury by inhibiting recruitment of monocyte lineage cells. Circulation 2004;110:2444–52.
[22] Channon KM, Qian HS, Youngblood SA, et al. Acute host-mediated endothelial injury after adenoviral gene transfer in normal rabbit arteries: impact on transgene expression and endothelial function. Circ Res 1998;82:1253–62.
[23] Varenne O, Gerard RD, Sinnaeve P, Gillijns H, Collen D, Janssens S. Percutaneous adenoviral gene transfer into porcine coronary arteries: is catheter-based gene delivery adapted to coronary circulation? Hum Gene Ther 1999;10:1105–15.
[24] Hiltunen MO, Laitinen M, Turunen MP, et al. Intravascular adenovirus-mediated VEGF-C gene transfer reduces neointima formation in balloon-denuded rabbit aorta. Circulation 2000;102:2262–8.
[25] Egashira K. Clinical importance of endothelial function in arteriosclerosis and ischemic heart disease. Circ J 2002;66:529–33.
[26] Griendling KK, FitzGerald GA. Oxidative stress and cardiovascular injury. Part II. Animal and human studies. Circulation 2003;108:2034–40.
[27] Selzman CH, Miller SA, Zimmerman MA, Gamboni-Robertson F, Harken AH, Banerjee A. Monocyte chemotactic protein-1 directly induces human vascular smooth muscle proliferation. Am J Physiol Heart Circ Physiol 2002;283:H1455–61.
[28] Fukuda D, Sata M, Tanaka K, Nagai R. Potent inhibitory effect of sirolimus on circulating vascular progenitor cells. Circulation 2005;111:926–31.
[29] Kitamoto S, Nakano K, Hirouchi Y, et al. Cholesterol-lowering independent regression and stabilization of atherosclerotic lesions by pravastatin and by antimonocyte chemoattractant protein-1 therapy in nonhuman primates. Arterioscler Thromb Vasc Biol 2004;24:1522–8.

tapraid4/zh4-ahea/zh4-ahea/zh400508/zh48209d08z | xppws | S=1 | 3/5/08 | 12:14 | MS: H-00986-2007 | Ini: 05/JTG/BEW

Am J Physiol Heart Circ Physiol 294: H000–H000, 2008.
First published _____; doi:10.1152/ajpheart.00986.2007.

Moderate hypothermia increases the chance of spiral wave collision in favor of self-termination of ventricular tachycardia/fibrillation

Masahide Harada,[1]* Haruo Honjo,[1]* Masatoshi Yamazaki,[1] Harumichi Nakagawa,[1] Yuko S. Ishiguro,[1] Yusuke Okuno,[1] Takashi Ashihara,[2] Ichiro Sakuma,[3] Kaichiro Kamiya,[1] and Itsuo Kodama[1]

[1]*Department of Cardiovascular Research, Research Institute of Environmental Medicine, Nagoya University, Nagoya;* [2]*Department of Cardiovascular Medicine, Shiga University of Medical Science, Otsu; and* [3]*Graduate School of Engineering, The University of Tokyo, Tokyo, Japan*

Submitted 27 August 2007; accepted in final form 23 February 2008

Harada M, Honjo H, Yamazaki M, Nakagawa H, Ishiguro YS, Okuno Y, Ashihara T, Sakuma I, Kamiya K, Kodama I. Moderate hypothermia increases the chance of spiral wave collision in favor of self-termination of ventricular tachycardia/fibrillation. *Am J Physiol Heart Circ Physiol* 294: H000–H000, 2008. First published _____; doi:10.1152/ajpheart.00986.2007.—In cardiac arrest due to ventricular fibrillation (VF), moderate hypothermia (MH, 33°C) has been shown to improve defibrillation success compared with normothermia (NR, 37°C) and severe hypothermia (SH, 30°C). The underlying mechanisms remain unclear. We hypothesized that MH might prevent reentrant excitations rotating around functional obstacles (rotors) that are responsible for the genesis of VF. In two-dimensional Langendorff-perfused rabbit hearts prepared by cryoablation (n = 13), action potential signals were recorded by a high-resolution optical mapping system. During basic stimulation (2.5–5.0 Hz), MH and SH caused significant prolongation of action potential duration and significant reduction of conduction velocity. Wavelength was unchanged at MH, whereas it was shortened significantly at SH at higher stimulation frequencies (4.0–5.0 Hz). The duration of direct current stimulation-induced ventricular tachycardia (VT)/VFs was reduced dramatically at MH compared with NR and SH. The spiral wave (SW) excitations documented during VT at NR were by and large organized, whereas those during VT/VF at MH and SH were characterized by disorganization with frequent breakup. Phase maps during VT/VF at MH showed a higher incidence of SW collision (mutual annihilation or exit from the anatomical boundaries), which caused a temporal disappearance of phase singularity points (PS-0), compared with that at NR and SH. There was an inverse relation between PS-0 period in the observation area and VT/VF duration. MH data points were located in a longer PS-0 period and a shorter VT/VF duration zone compared with SH. MH causes a modification of SW dynamics, leading to an increase in the chance of SW collision in favor of self-termination of VT/VF.

optical mapping; ventricular fibrillation

SUCCESSFUL USE OF THERAPEUTIC hypothermia after cardiac arrest in humans was described in the late 1950s as a procedure to improve the clinical outcomes but then almost abandoned because of uncertain benefits and difficulties with its use (17). It was demonstrated in 2002 by two prospective randomized trials that the induction of therapeutic hypothermia in patients, who had been resuscitated after cardiac arrest due to ventricular fibrillation (VF), increased neurological recovery and reduced mortality (2, 12a). This has led to recent guideline recommendations that all unconscious adult patients with spontaneous circulation after out-of-hospital cardiac arrest should be cooled to 32–34°C for 12–24 h when the initial rhythm was VF (1). In experiments using swines with induced VF, Boddicker et al. (3) demonstrated that defibrillation success of electrical shocks and resuscitation outcomes were significantly improved under moderate hypothermia (MH, 33°C) compared with normothermia (NR, 37°C) and that the benefit of MH was larger than severe hypothermia (SH, 30°C) (3). The underlying mechanisms of this amelioration are not well understood. Temperature-dependent amelioration of ischemic myocardial injury may contribute to the beneficial effect of hypothermia for resuscitation, but this does not explain an advantage of MH over SH (10). Defibrillation success or failure depends on the balance between shock-induced extinction and the generation of such rotors (9). We hypothesized that MH may have substantial effects on the rotor dynamics in favor of its termination. To test this hypothesis, we investigated temperature-dependent modification of spiral wave (SW) dynamics in a perfused two-dimensional (2-D) layer of rabbit ventricle by using our custom-made, high-resolution optical action potential mapping system.

METHODS

Experimental model. The protocol was approved by the Institutional Animal Care and Use Committee at Nagoya University. Experiments were performed in hearts from Japanese White rabbits of both sexes weighing ~1.7–2.0 kg (n = 13). The experimental model is essentially the same as reported previously (26). In brief, rabbits were anesthetized with pentobarbital sodium (~10–15 mg/kg), and the hearts were rapidly removed. The isolated hearts were continuously perfused on a Langendorff apparatus with modified Krebs-Ringer solution equilibrated with 95% O_2-5% CO_2 to maintain pH at ~7.3–7.4. Complete atrioventricular (AV) block was produced by ligation of His bundle. Two-dimensional epicardial layer of ventricular myocardium (1.0 ± 0.2 mm thick) was created by cryoprocedure. At the end of experiment, the thickness of surviving epicardial myocardium was confirmed by staining the heart with 2,3,5-triphenyltetrazolium chloride. This model has an advantage over intact three-dimensional (3-D) heart to visualize the SW reentry on the epicardial surface.

High-resolution optical mapping. The optical mapping system used in this study is similar to that described previously, except for inducing the upgraded digital video camera (26). After endocardial freezing, the hearts were stained with a voltage-sensitive dye, 4-{β-[2-(di-*n*-butylamino)-6-naphthyl]vinyl}pyridinium. To mini-

* M. Harada and H. Honjo contributed equally to this work.

Address for reprint requests and other correspondence: I. Kodama, Dept. of Cardiovascular Research, Research Inst. of Environmental Medicine, Nagoya Univ., Furo-cho, Chikusa-ku, Nagoya, 464-8601, Japan (e-mail: ikodama@riem.nagoya-u.ac.jp).

The costs of publication of this article were defrayed in part by the payment of page charges. The article must therefore be hereby marked "*advertisement*" in accordance with 18 U.S.C. Section 1734 solely to indicate this fact.

tapraid4/zh4-ahea/zh4-ahea/zh400508/zh48209d08z | xppws | S=1 | 3/5/08 | 12:14 | MS: H-00986-2007 | Ini: 05/JTG/BEW

mize motion artifacts, 15 mM 2,3-butanedione monoxime (BDM) was added unless otherwise specified. Bipolar electrograms were recorded through widely spaced electrodes to monitor the whole ventricular excitations. The signals were filtered from 1.5 to 1,000 Hz and digitized at 1,000 Hz.

The hearts were illuminated with bluish-green light-emitting diodes; the emitted fluorescence was recorded with a solid-state image-sensing digital video camera (Fastcam-Max, Photron, Japan) to acquire 10-bit grayscale images from 256 × 256 sites simultaneously at a speed of 1,000 frames/s. The images acquired (30 × 30 mm) covered the anterolateral surface of the left ventricle (LV). Each acquisition lasted for 2–10 s.

To reveal the action potential signal, the background fluorescence was subtracted from each frame and low-pass spatial filtering was applied. Action potential configuration was analyzed after the application of a five-point median filter to the spatially averaged data, and the data were then normalized to the range of the maximum and the minimum values in the respective 800-frame sample. A time point at 10% depolarization in the upstroke phase and a time point at 90% repolarization in its repolarization phase were identified for each action potential signal, and the interval was measured as action potential duration at 90% repolarization (APD_{90}). Wave-front tail dynamics during ventricular tachycardia (VT)/VF were visualized by connecting the 10% depolarization points in the action potential upstrokes as the wave front (red) in the recording area and by connecting the 90% repolarization points at the wave tail (green). The wave propagation pattern during VT/VF was quantified with the aid of the phase-mapping methods described by Gray et al. (12). Phase singularity (PS) was defined as the point at which all phases converged.

Myocardial cooling of heart. The heart was sequentially cooled from 37°C (NR) to 33°C (MH), and then to 30°C (SH) by controlling temperature of the perfusate and thermoregulated water chamber. The target temperature was decided in accordance with the in vivo experimental study by Boddicker et al. (3). We confirmed in pilot experiments of five rabbit hearts that the surface temperature of LV free wall monitored by thermography (TVS-200 Nippon Avionics, Tokyo) was kept homogeneous at the respective target temperature (Fig. 1), and the effects of cooling on the basal electrophysiological properties reached a steady state at ~10 min. The cooling-induced changes were reversible upon rewarming to NR.

Experimental protocols. Steady-state APD and its distribution were measured under constant stimulation (S1) from the LV apex at basic cycle length (BCL) of 200–400 ms. Effective refractory period (ERP) was estimated at the LV apex by a standard extrastimulus (S1-S2) protocol at BCL of 400 ms. Steady-state conduction velocity (CV) was measured under S1 stimulation at the center of LV free wall at BCL of 200–400 ms. A monopolar electrode made of platinum wire (diameter, 0.5 mm) was used for stimulation. The pulses applied were 2 ms in duration and 1.2 times the diastolic threshold for S1 and twice the diastolic threshold for S2.

CV was measured in a square (24 × 16 mm) around the stimulation site at the center of the LV free wall. The longitudinal and transverse directions (LD and TD) of propagation were determined from the activation maps elicited by S1 stimulation. The long and short axes of the CV measurement square were set parallel to LD and TD, respectively. CVs in LD (CV_L) and TD (CV_T) were calculated from the slope of a linear least-square fit of the activation time plotted against the distance.

We used the dynamic pacing method to characterize the restitution properties of APD and CV (15). With regard to APD, the LV apex was initially paced at a BCL of 500 ms, and the BCL was progressively shortened in steps of 10–100 ms. A minimum of 60 stimuli were delivered at a given BCL. APD restitution at a site of 3 mm distant from the stimulation site on the anterior LV free wall was analyzed. The APD_{90} of the last two paced action potentials was measured, and the differences >5 ms was defined as APD alternans. The BCL was shortened until either a 2:1 block or higher-order periodicity occurred. The APD restitution curve was constructed by plotting APD_{90} against the preceding diastolic interval, and the curve was fitted to a single exponential function (ORIGIN 7.0, Microcal Software, Northampton).

To evaluate the CV restitution, the center of the LV free wall was initially paced at a BCL of 700 ms, and the BCL was progressively shortened in steps of 10–200 ms. A minimum of 60 stimuli were delivered at a given BCL. CV_L and CV_T in the 24 × 16 mm^2 around the stimulation site were measured for the last 10 excitations from the time-distance plots and then averaged. The restitution curves of CV_L and CV_T plotted as a function of BCLs were fitted to a single exponential function, and they were characterized by measuring "breadth" and "depth" (5). The breadth was defined as the BCL range corresponding to CV recovery of 90% or less. The depth was defined as the CV range between the minimum value and 90% recovery.

VT/VF resulting from SW excitation was induced by modified cross-field stimulation. Eighteen S1 stimuli at a BCL of 400 ms were applied to the LV apex through a pair of contiguous bipolar electrodes. A 10-ms monophasic rectangular pulse of constant voltage (10–20 V) was generated by a direct current (DC) power unit and delivered from the unit through a 6,700-pF capacitor connected to a power MOS-FET switch. A pair of Ag-AgCl paddle electrodes (7 mm in diameter) was placed on the lateral surface of both ventricles for the DC stimulation (DS2) to induce an electrical filed in a direction roughly perpendicular to the S1 excitation from the apex (26). The S1-DS2 coupling interval was shortened progressively in 10-ms steps to cover the whole vulnerable window of the final S1 excitation at the respective temperature (from 100 ms longer than ERP until reaching

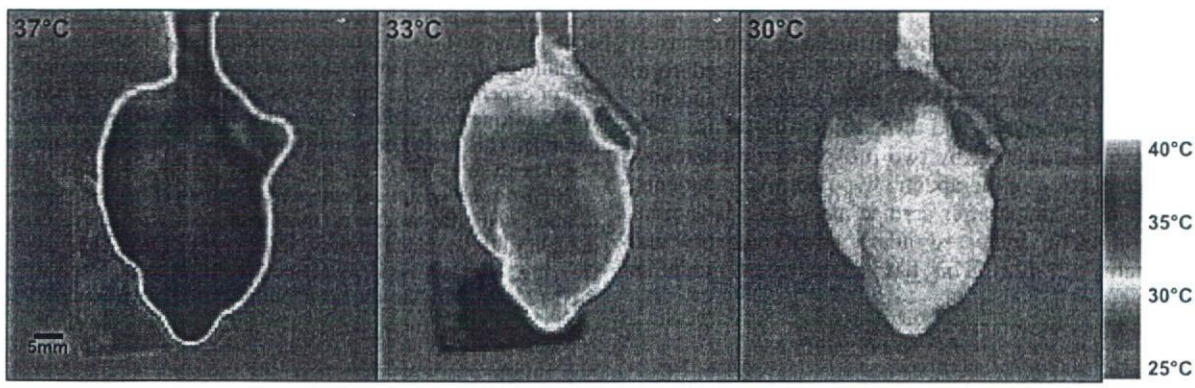

Fig. 1. Thermography images of a heart at normothermia (NR, 37°C), moderate hypothermia (MH, 33°C) and severe hypothermia (SH, 30°C). The temperature images recorded by thermography are shown as color gradients, ranging from red (40°C) to light blue (25°C).

COLOR

tapraid4/zh4-ahea/zh4-ahea/zh400508/zh48209d08z | xppws | S=1 | 3/5/08 | 12:14 | MS: H-00986-2007 | Ini: 05/JTG/BEW

the loss of ventricular capture). The sequence was repeated in each heart at three stages of DS2 intensity (10, 15, and 20 V). The incidence of VT/VFs was presented as percentage of the episodes over the number of DS2 applied.

Statistical analysis. Group data were expressed as means ± SD. Statistical comparisons were performed by ANOVA with multiple comparison, *t*-test, or χ^2 test when appropriate. Differences were considered significant when the probability value was <0.05.

RESULTS

Basal electrophysiological properties. Representative changes in APD under constant stimulation (BCL, 400 ms) are shown in Fig. 2*A*; APD_{90} values in the entire mapping area are displayed as color gradients (*left*), and action potential signals obtained from 16 sites covering 18 × 18 mm^2 are superimposed (*right*). Figure 2*B* summarizes the temperature-dependent changes in APD_{90} values. When APD alternans was induced at shorter BCLs, the shorter and longer APD_{90} values were averaged. Cooling to 33°C (MH) and 30°C (SH) resulted in an almost homogeneous prolongation of APD. APD_{90} values at a BCL of 400, 250, and 200 ms were increased significantly by 11–30% at MH and by 13–43% at SH. The dispersion of APD_{90} among the 16 recording sites at BCL of 400 ms was slightly increased from 18 ± 3 ms at NR to 22 ± 4 ms at MH (not significant) and 25 ± 6 ms at SH ($P < 0.05$ vs. NR). ERP at 400 ms was increased in parallel with APD_{90}, from 149 ± 18 ms at NR to 182 ± 17 ms at MH ($P < 0.05$ vs. NR) and to 203 ± 23 ms at SH ($P < 0.05$ vs. NR).

In experiments to examine conduction properties, the isochrones of activation front exhibited a smooth, symmetric, elliptical pattern; the long axis corresponded to the fiber orientation of subepicardial cardiac muscle. MH and SH caused significant reduction of both CV_L and CV_T in steps (Fig. 2*C*). The reduction of CVs at SH was enhanced at shorter BCLs, and the enhancement was more prominent in CV_T than in CV_L (Fig. 2*C*), giving rise to an increase of the anisotropic ratio (CV_L/CV_T) at a BCL of 200 ms from 1.9 ± 0.3 for NR to 2.1 ± 0.6 for MH (not significant) and to 3.5 ± 1.6 for SH ($P < 0.05$ vs. NR).

We estimated wavelength ($WL = APD_{90} \times CV$) during constant pacing (Fig. 2*D*). At a BCL of 400 ms, both WL_L and WL_T at MH and SH were significantly longer than those at NR. In contrast, at BCL of 250 and 200 ms, WL_L and WL_T at SH were significantly shorter than those at NR and MH.

We used the dynamic pacing method to characterize the restitution properties. The maximal APD restitution slopes at MH and SH were larger than that at NR (see supplemental Fig. 1*A* and supplemental Table 1; note: all supplemental material may be found with the online version of his article). With

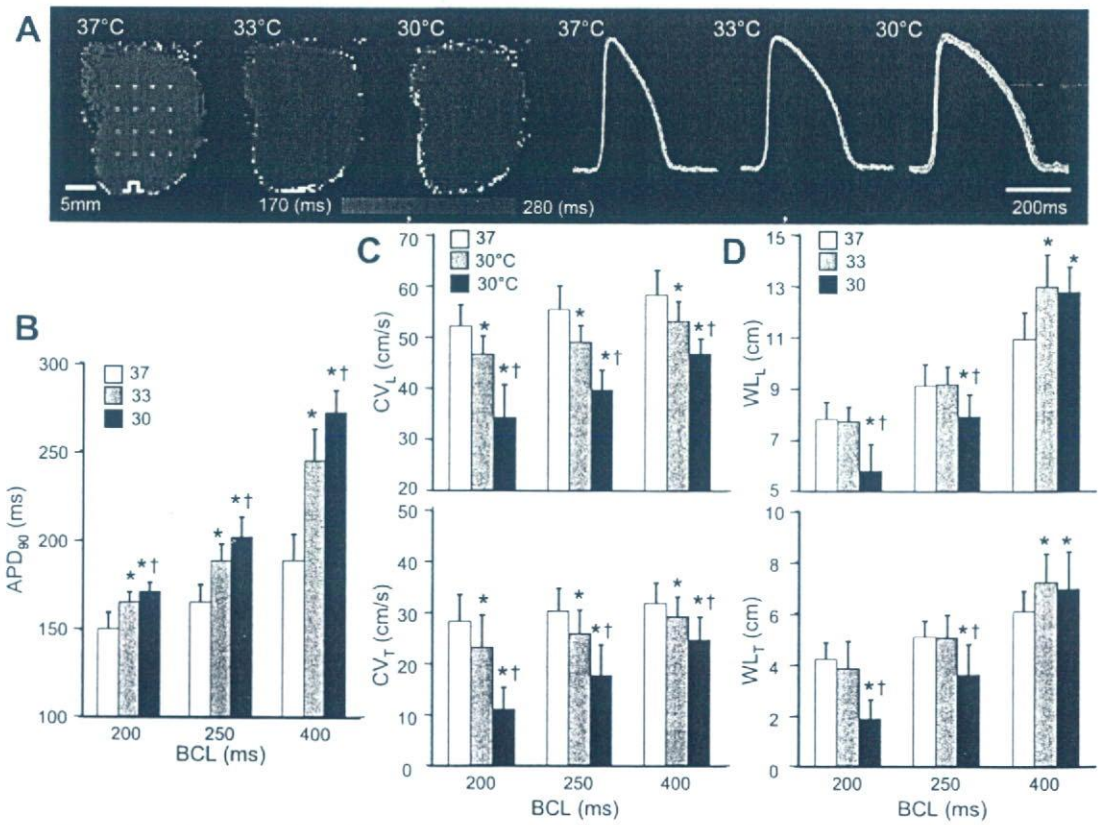

Fig. 2. Basal electrophysiological properties. *A*: action potential duration at the 90% polarization (APD_{90}) in the recording area (anterolateral surface of left ventricular free wall) under constant stimulation from apex [basic cycle length (BCL) of 400 ms]. *A*, *left*: APD_{90} color gradient maps, ranging from red (shortest) to blue (longest). *A*, *right*: superimposed action potential signals (BCL, 400 ms) recorded from the 16 sites covering 18 × 18 mm area (white dots in the left-end map). *B*: APD_{90} at BCL of 200, 250, and 400 ms (means ± SD, $n = 6$). *C*: conduction velocity in longitudinal (CV_L; *top*) and transverse (CV_T; *bottom*) directions at BCL of 200, 250, and 400 ms (means ± SD, $n = 6$). *D*: wave length during longitudinal (WL_L; *top*) and transverse (WL_T; *bottom*) propagation at BCL of 200, 250, and 400 ms (means ± SD, $n = 6$). *$P < 0.05$ vs. 37°C; †$P < 0.05$ vs. 33°C.

COLOR

tapraid4/zh4-ahea/zh4-ahea/zh400508/zh48209d08z | xppws | S=1 | 3/5/08 | 12:14 | MS: H-00986-2007 | Ini: 05/JTG/BEW

regard to CV restitution, the breadth and depth (5) were unchanged or increased slightly at MH, whereas they were increased largely by two- to threefold at SH (supplemental Fig. 1*B* and supplemental Table 1).

VT/VFs induced by DC stimulation. The VT/VFs induced in 13 hearts by DS2 were categorized into two types in terms of their duration: *1*) nonsustained, lasting ≥5 beats and <30 s and F3 *2*) sustained, lasting ≥30 s (Fig. 3*A*). In terms of ECG morphology (distant bipolar electrogram), VT was categorized into monomorphic type and polymorphic type. In the present experiments, polymorphic VT lasting ≥30 s was defined as VF. At NR, 71 VT/VFs were induced by 241 DS2s (total incidence, 29%): 59 (83%) were nonsustained (46 monomorphic and 13 polymorphic), and 12 (17%) were sustained (all monomorphic). At MH, 108 VT/VFs were induced by 289 DS2s (total incidence 37%): 107 (99%) were nonsustained (all polymorphic VTs), and 1 (1%) was sustained (VF). At SH, 89 VT/VFs were induced by 203 DS2s (total incidence 44%): 78 (88%) were nonsustained (all polymorphic VTs), and 11 (12%) were sustained (all VFs). There were no significant differences among the three temperature conditions in the average intensity of DS2 to induce VT/VFs (16.0 ± 3.7 at NR, 15.2 ± 3.9 at MH, and 14.8 ± 3.8 V at SH, $P = 0.14$). Thus, although the total incidence of VT/VFs was increased in steps by cooling (Fig. 3*A*), the relative incidence of sustained form over the total VT/VF episodes was decreased dramatically at MH ($P < 0.001$) (Fig. 3*B*).

Dynamics of SW excitation. Optical images of excitation during VT/VF were analyzed in 10 hearts exhibiting visible SWs at NR as well as at MH and SH. At NR, some forms of SW excitation (single-loop or figure-eight reentry) were documented in 17 episodes (59%) of 29 VTs available for image analysis. The remaining 12 VTs showed one-way propagation of wave fronts traversing the observation area. At MH and SH, multiple SW excitations were always (100%) documented in 32 and 46 VT/VF episodes, respectively.

Figure 4 shows representative isochrone maps. In the record F4 at NR (Fig. 4*A*), a clockwise rotation of wave front around a line of functional block (FBL, ~3.0 mm) can be seen at a cycle length (CL) of 146–148 ms. The circuit was stable for >30 s and exhibited a small meandering. Distant bipolar electrogram (ECG) showed monomorphic ventricular excitations. Action potential signals (*sites a–d*) showed regular configurations with no isoelectric segments, and there were clear double potentials on the FBL (*site e*) as reported previously (26).

Figure 4*B* shows activation patterns during a short polymorphic VT (lasting for 5 s) at MH. SWs changed their circuits in a beat-to-beat manner with CLs varying from 153 to 224 ms. In *beat i*, there were two reentry circuits. In the upper region, a wave front coming down from the base faced a long FBL, giving rise to its extension toward the center to maintain the clockwise rotation. In the lower region, a wave toward the right margin was divided into two pathways of counterrotation around a long tortuous FBL. The upper limb of this lower circuit shared a common pathway with the lower limb of the upper circuit. The lower circuit ended by collision at the opposite side of the FBL. In *beat ii*, a single clockwise rotation remained around a Y-shaped FBL. In *beat iii*, double circuits appeared again around two long L-shaped FBLs. The wave fronts finally terminated by collision (*sites c* and *e*). The action potentials recorded from the circuits showed substantial beat-to-beat variation, and some of them had very long durations.

Figure 4*C* shows more complex activation patterns during VF (lasting ≥30 s, CL varying from 124 to 216 ms) at SH. In *beat i*, a wave front of counterclockwise rotation passed through between two curved FBLs near the apex and then merged with another wave front coming down from the left upper region, resulting in two wave fronts of opposite direction. In *beat ii*, the opposite wave fronts created an additional very-long FBL, and several wave fronts coexisted around three FBLs. In *beat iii*, the multiple wave fronts merged with each other around the center, giving rise to a labyrinth associated with collision (*site d*). The action potential signals recorded from the circuits showed tremendous beat-to-beat changes.

The modification of SW dynamics by cooling was investigated more extensively by phase mapping analysis. At NR, SW excitations terminated spontaneously when the two PSs of opposite chirality collided with each other (mutual annihilation) or when the PS collided against an anatomical boundary (AV groove), but the chance was rare as reported previously (26). At MH, the chance of collision was increased because of large meandering and further generation of new PSs. Figure 5*A* F5 shows SW extinction patterns in the final beat of a VT episode (the same experiment as in Fig. 4*B*). A PS of clockwise rotation

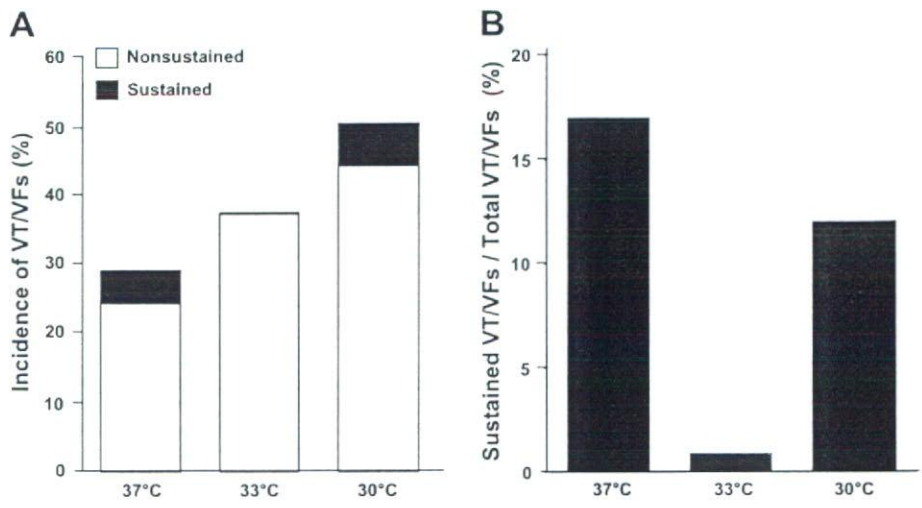

Fig. 3. Incidence and duration of shock-induced ventricular tachycardia (VT)/ventricular fibrillation (VF). *A*: total incidence of VT/VFs induced by direct current (DC) stimulation (DS2) in 13 hearts at 37°, 33°, and 30°C. The VT/VFs were categorized into 2 types; nonsustained (≥5 beats, <30 s), and sustained (≥30 s). *B*: percentage of sustained VT/VFs over total VT/VFs.

tapraid4/zh4-ahea/zh4-ahea/zh400508/zh48209d08z | xppws | S=1 | 3/5/08 | 12:14 | MS: H-00986-2007 | Ini: 05/JTG/BEW

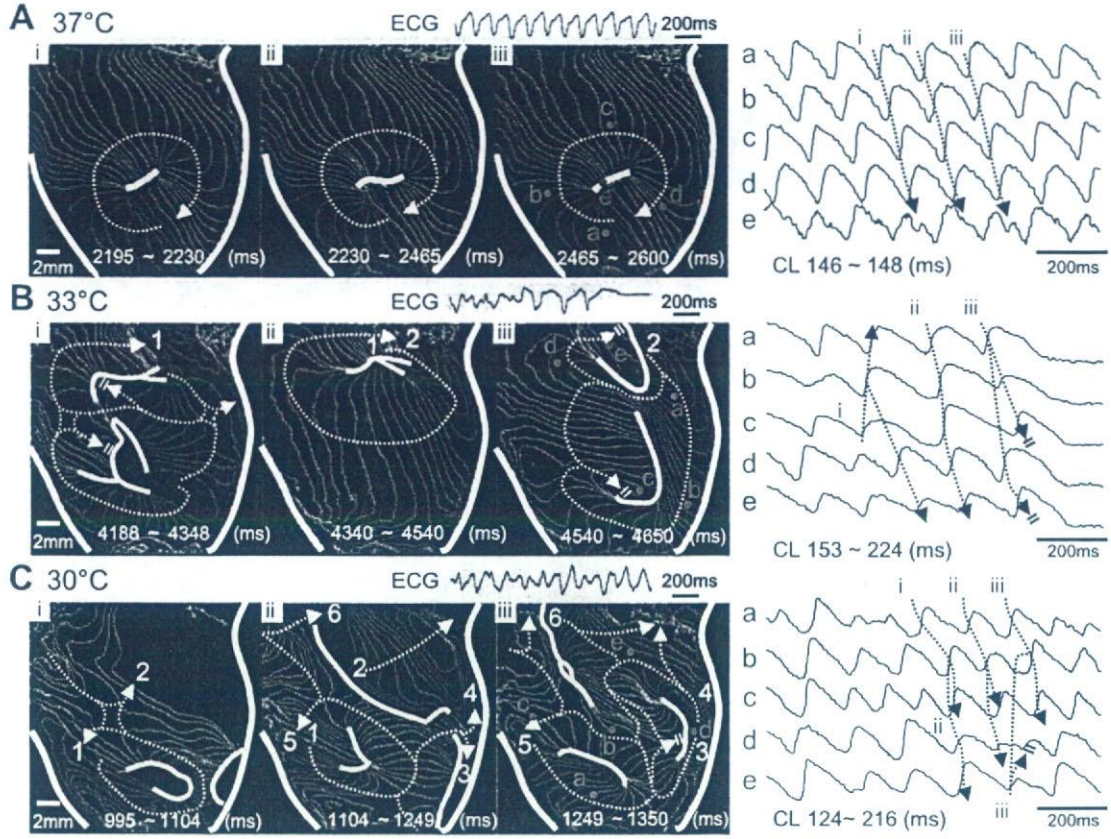

Fig. 4. Spiral wave (SW) excitations during DC stimulation-induced VT/VF. *A*: isochrone maps of 3 consecutive activations during sustained monomorphic VT at 37°C (4-ms intervals, blue lines for earlier wave fronts, green lines for later wave fronts). Clockwise rotation around a line of functional block (FBL, yellow) in the anterior left ventricular free wall was repeated at a cycle length (CL) of 146 to 148 ms. *A–C*, *top*: distant bipolar electrogram (ECG) during the VT. *A–C*, *right*: optical action potential signals from 5 sites (*sites a–e* in the isochrone map of *beat iii*). *B*: isochrone maps of 3 activations during nonsustained polymorphic VT at 33°C. Single or multiple SW excitations circulated around FBLs with marked beat-to-beat variations (CLs varied from 153 to 224 ms). *C*: isochrone maps of 3 activations during sustained VF at 30°C. Multiple SWs circulated around more complex FBLs with tremendous beat-to-beat variations (CLs varied from 124 to 216 ms). All the records of *A–C* were obtained from the same heart. Numbers on the white dotted arrows in isochrone maps (*B* and *C*) indicate the connection of respective activation waves.

(PS1) moved back and forth in the middle upper region of LV (4,570–4,592 ms). A pair of new PSs of opposite chirality (PS2 and PS3) was then generated (4,592 ms) due to front-tail interactions (supplemental Fig. 2*A*). The distance between the two PSs initially increased and then decreased, culminating in mutual annihilation. After considerable meandering, PS1 was finally pushed out of the AV groove (supplemental movie 1). The trajectories of three PSs were plotted on 2-D (x-y) axes (Fig. 5*B*) as well as on 3-D (x-y-time) axes (Fig. 5*C*).

Figure 6*A* shows four sequential phase maps of a VF episode (the same experiment as in Fig. 4*C*). There were six PSs at 2,232 ms. A pair of counterrotating PSs in the central region (PS1, PS2) approached each other to a very close distance (2,250 ms) and then separated without mutual annihilation, and the sequence was repeated (supplemental Fig. 2*B* and movie 2). F6 Figure 6*B* illustrates trajectories of the 11 PSs in 2-D (x-y) axes. PS4, PS5, and PS6 were pushed out of the observation area after meandering. Two pairs of counterrotating PSs (PS3–PS11 and PS9–PS10) dissipated at last by mutual annihilation. PS1, PS2, PS7, and PS8 survived the period. Figure 6*C* shows 3-D time-space (x, y) plots of the trajectories of PS1 and PS2. The distance between PS1 and PS2 was plotted against time in Fig. 6*D*. The two PSs approached each other twice to a distance of ~0.5 mm but survived without annihilation. This behavior contrasts with the SW dynamics at MH, causing mutual annihilation easily.

We compared the closest distance (D_c) between a pair of counterrotating PSs constructing figure-eight reentry without mutual annihilation at MH and SH. Average values of D_c at SH were significantly less than those at MH (0.5 ± 0.2 vs. 1.3 ± 0.6 mm, $n = 6$, $P < 0.05$).

PS dynamics and VT/VF termination. We analyzed the PS dynamics more quantitatively to elucidate their roles in perpetuation and termination of rotors. Figure 7*A*, *left*, shows F7 representative changes in PS number during 2,000 frames (2 s) of VT/VF episodes. At NR, the number of PSs was normally 1 and, rarely, increased to 2 for short periods. At MH and SH, the number of PSs increased frequently to ~2–8, resulting in an increase of average PSs/2 s. Pooled data are summarized in Fig. 7*A*, *right*.

In Fig. 7*A*, *left*, it was also evident that temporal PS dissipation from the observation area (PS-0 period) occurred more frequently at MH than at NR and SH. Such temporal PS dissipation would favor spontaneous termination of VT/VF depending on rotors. We, therefore, plotted the duration of 78 VT/VF episodes at MH and SH against the respective total

tapraid4/zh4-ahea/zh4-ahea/zh400508/zh48209d08z | xppws | S=1 | 3/5/08 | 12:14 | MS: H-00986-2007 | Ini: 05/JTG/BEW

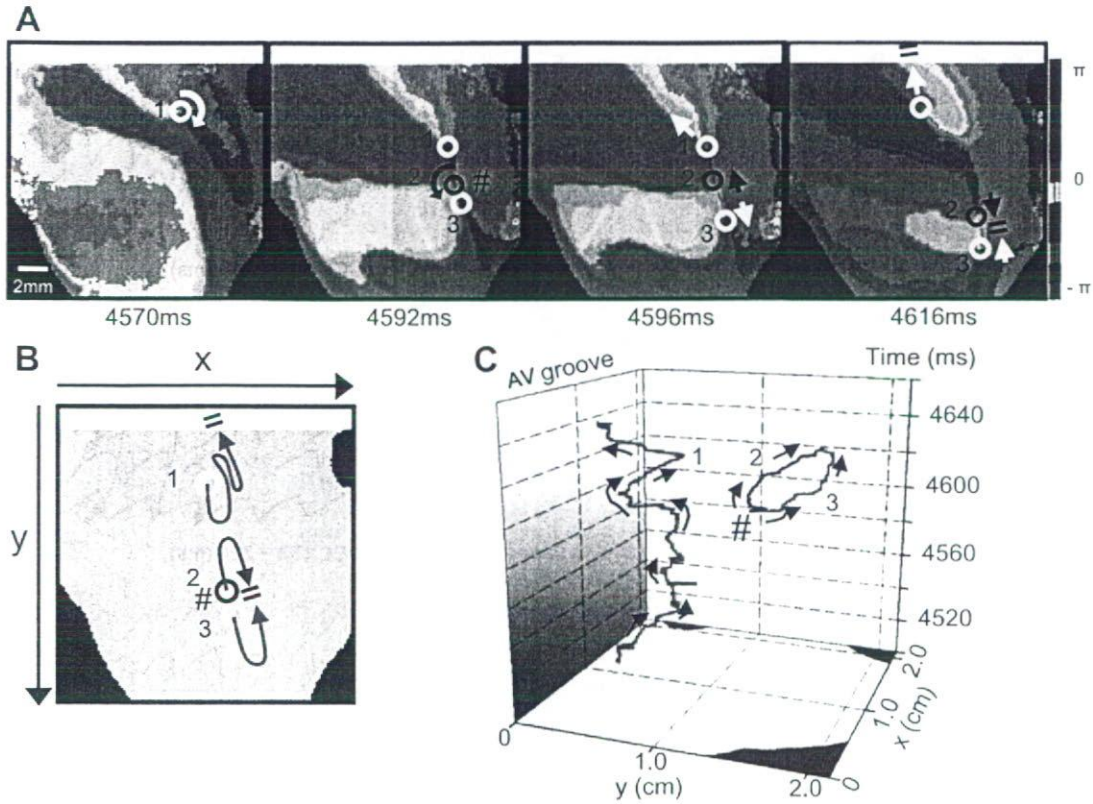

Fig. 5. Self-termination of SW reentry at 33°C. *A*: 4 snapshots of phase maps of the final beat of a short polymorphic VT episode (the same experiment as in Fig. 4*B*). Phase singularities (PSs) are indicated by circles (white for clockwise rotation; black for counterclockwise rotation). A pair of new PSs (PS2 and PS3) were generated from a SW excitation circulating around PS1 via front-tail interactions causing breakup (#). PS2 and PS3 terminated soon by mutual annihilation, whereas PS1 terminated by collision with atrioventricular (AV) groove after meandering. *B*: trajectories of the 3 PSs on two-dimensional (2-D) (x, y) axes (red for clockwise rotation; blue for counterclockwise rotation). *C*: trajectories of the 3 PSs plotted on space (x, y) and time axes. The half-tone wall on the left indicates AV groove.

PS-0 period/2 s (Fig. 7*B*). There was an inverse relation between the two parameters. MH data points were located in a longer PS-0 period and shorter VT/VF duration zone compared with SH.

Spatial excitable gap during SW excitation. The basal electrophysiological data at short BCLs (200–250 ms) showed that WLs at SH were significantly shorter than those at MH and NR (Fig. 2*D*). This seems to suggest that WLs during rotation of SW at SH are short, allowing a relatively wide excitable gap. During SW reentry, however, both APD and CV are influenced by wave-front curvature, which increases progressively toward the rotation center (19). We, therefore, estimated the spatial excitable gap (SEG) of SW by measuring an area circumscribed by wave front, wave tail, and an arc of a certain radius (distance) from the SW tip. Representative results are shown in Fig. 8*A*. At NR, there was a dynamic variation of SEG during a single rotation; the value at 0.5 mm from the rotation center ranged from 0.11 to 0.43 mm^2. SEG of SW at MH showed a similar variation, although the measurements did not cover a full rotation due to meandering of the circuit. SEG of SW at SH was characterized by a less variation with a larger minimal value (0.27 mm^2 at 0.5 mm). Figure 8*B* compares the minimal SEG (SEG_{min}) of six hearts (for a distance at 0.5 mm). SEG_{min} at SH was significantly larger than those at NR and MH for a distance of 0.5–1.0 mm, whereas there were no significant differences among the three temperatures for a distance $\geq$ 2.0 mm (1.8 $\pm$ 0.9 at NR, 1.3 $\pm$ 0.4 at MH, and 2.0 $\pm$ 0.6 mm^2 at SH, for a distance of 2.0 mm, $P = 0.12$). This behavior at SH would help SWs form small circuits and coexist without mutual annihilation.

DISCUSSION

The major findings in the present study are as follows. First, MH and SH caused a significant prolongation of APD and a reduction of CV; WL was unchanged at MH, whereas it was shortened at SH at higher stimulation frequencies. Second, the duration of VT/VFs was reduced dramatically at MH compared with that at NR and SH. Third, SWs were destabilized at MH and SH with different behaviors; those at MH were characterized by more frequent collisions, leading to longer temporal disappearance of PSs (PS-0) in favor of self termination, compared with those of SH.

Cooling-induced changes in the basal electrophysiological properties. The temperature-dependent prolongation of APD and the reduction of CV in response to cooling are the well-known properties of cardiac muscle. More than several mechanisms are involved in the APD prolongation. Voltage-clamp studies have indicated that the major factor is a decrease in the delayed rectifier K^+ current (I_K) with a temperature coefficient

tapraid4/zh4-ahea/zh4-ahea/zh400508/zh48209d08z | xppws | S=1 | 3/5/08 | 12:14 | MS: H-00986-2007 | Ini: 05/JTG/BEW

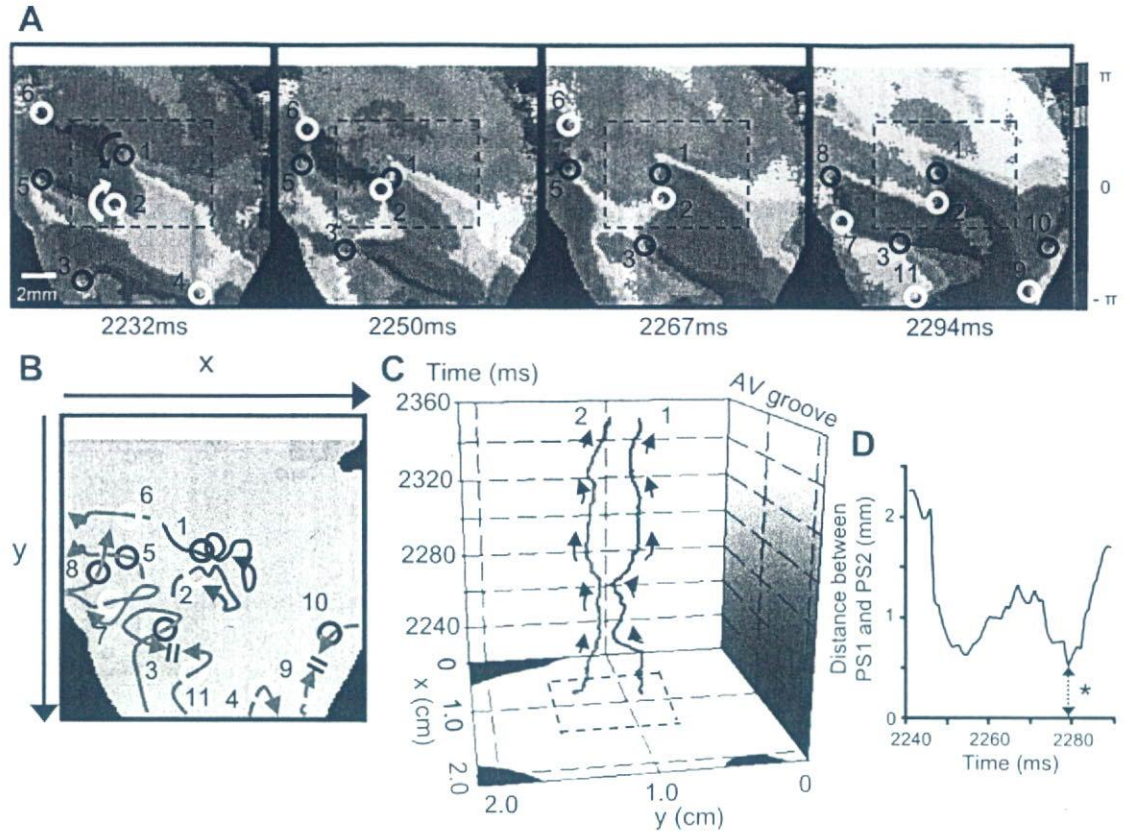

Fig. 6. Coexistence of multiple SW excitations at 30°C. *A*: 4 snapshots of phase maps during an episode of sustained VF (the same experiment as in Fig. 4C). Eleven PSs were recognized in the observation area (white for clockwise rotation; black for counterclockwise rotation). *B*: trajectories of the 11 PSs on 2-D (x, y) axes. Some of them were pushed out of the observation area after meandering (PS4, PS5, and PS6) or dissipated by mutual annihilation (PS3–PS11, and PS9–PS10), but others (PS1, PS2, PS7, and PS8) survived the period. *C*: trajectories of the 2 PSs (PS1 and PS2) in the central dotted square were plotted on space (x, y) and time axes (red for clockwise rotation; blue for counterclockwise rotation). *D*: temporal change in the distance between PS1 and PS2. *Closest distance.

(Q_{10}) of 4.4 (14). The decrease of I_K is the result in part of its delayed activation (14). Delayed inactivation of L-type Ca^{2+} current (Q_{10} of 2.3) and a decrease of inward rectifier K^+ current (Q_{10} of 1.5) contribute as well to the APD prolongation (6, 14). A decrease of time-independent outward current has also been described (14). The reduction of CV is most likely explained by a decrease of Na^+ current availability via its temperature-dependent slowing of activation/inactivation kinetics (Q_{10} of ~3) (13). A reduction of gap junction conductance (Q_{10} of 1.4) by cooling may also contribute to the CV reduction (4).

Destabilization of rotor dynamics: undesirable or beneficial? Hypothermia caused temperature-dependent destabilization of SW dynamics. This may be attributed in part to a steeper slope of APD restitution engaged with increased depth and breadth of CV restitution, which is known to cause an enhancement of wave-front tail interactions (25). Nevertheless, we cannot rule out other factors affecting SW stability; those include short-term cardiac memory, electrotonic current, and intracellular Ca^{2+} cycling (24). The effect of cooling on these latter factors remains to be quantified. In any case, an increased dynamic instability would favor the generation of functional reentry. Our results are consistent with this prediction since the total incidence of VT/VF elicited by DC stimulation was increased in steps from NR to MH and SH.

Another consequence of enhanced dynamic instability is the destruction of existing waves, promoting self-termination of VT/VF. The mechanisms of SWs termination by an interaction with other waves were first demonstrated by Davidenko et al. (8). In a theoretical study on myocardial tissue model of finite size, Qu (20) has demonstrated that an increase of dynamic instability created by steep APD restitution slope promotes wave breaks, maintaining fibrillation, but it also causes the waves to extinguish, facilitating spontaneous termination of fibrillation. They showed three ways by which a wave self-terminates: *1*) two waves can annihilate each other if their tips collide, *2*) a wave can run into a region of refractoriness from a previous wave, or *3*) a wave can move off a tissue boundary (20).

In the present study, the relative incidence of sustained VT/VF over the total VT/VF episodes at MH was much less than those at NR and SH, indicating considerable promotion of self-termination at MH. In the phase maps, the average number of PSs/2 s was increased in steps with cooling, reflecting a more frequent generation of new SWs. However, the PS-0 period resulting from temporal dissipation of SWs was also increased especially at MH. Therefore, the promotion of self-termination of VT/VF at MH is explained most likely by an increased dissipation of existing SWs, which offsets the increased generation of new SWs.

COLOR

tapraid4/zh4-ahea/zh4-ahea/zh400508/zh48209d08z | xppws | S=1 | 3/5/08 | 12:14 | MS: H-00986-2007 | Ini: 05/JTG/BEW

COLOR

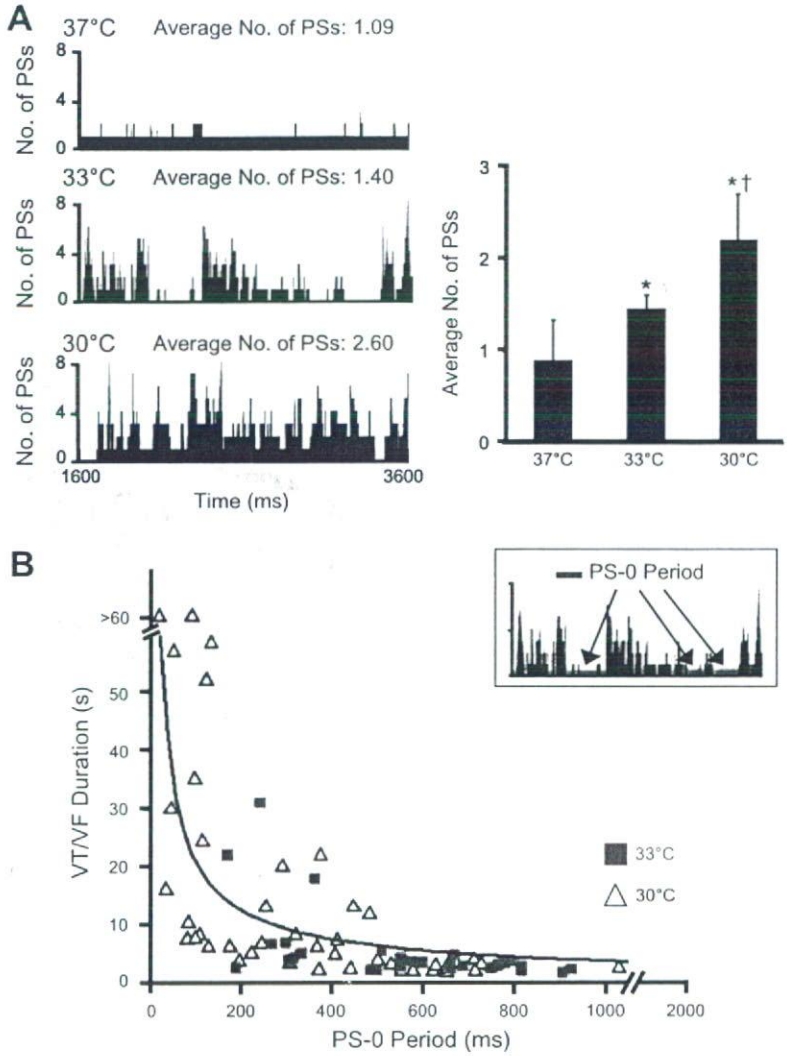

Fig. 7. PS dynamics and VT/VF duration. *A*: representative changes in PS number during 2,000 frames (2 s) of VT/VF episodes and averaged number of PSs/2 s at 37°, 33°, and 30°C (means ± SD, $n = 6$, $^*P < 0.05$ vs. 37°C, $\dagger P < 0.05$ vs. 33°C). *B*: relationship between temporal PS dissipation (total PS-0 period/2 s) and VT/VF duration. Seventy-eight VT/VF episodes (32 at 33°C, and 46 at 30°C) were analyzed. The data points were fitted by an exponential curve.

The dissipation of existing rotors at MH was the result of either mutual annihilation of 2 PSs or a collision of PSs with the AV groove after considerable meandering. Such dissipation of existing SWs was less frequent at SH. This may be the consequence of substantial shortening of WL at SH, reflected in the less value of the critical distance (D_c) between a pair of counterrotating PSs without mutual annihilation. Under constant stimulation at a long BCL (400 ms), WLs at MH and SH were both increased compared with NR, reflecting hypothermia-induced APD prolongation. At shorter BCLs (250 and 200 ms), however, WLs at MH were similar to NR because of the concomitant decrease of CV; WLs at SH were shortened significantly because of more pronounced reduction of CV. In the SW excitations during VT/VF, the SEG_{min} at MH close to the rotation center (≤1 mm) was comparable with NR, whereas the value at SH was significantly larger than NR and MH, suggesting a substantial shortening of WLs. However, the values at a distance ≥ 2.0 mm did not differ among the three temperature conditions. Smaller SEG_{min} at a distance ≤ 1 mm at NR and MH would facilitate wave-front tail interaction just around the rotation center, whereas larger SEG_{min} at SH would prevent it. However, these values would not affect the whole dynamics of SW excitations at a distance ≥ 2.0 mm. Wave-front tail interactions at a distance away from the core, causing SW destabilization at MH and SH, may be attributable to other factors, including restitution kinetics, cardiac memory, or Ca^{2+} dynamics (24).

In short, the hypothermia-induced enhancement of dynamic instability may have dual effects: an increase of ventricular vulnerability on one side and a destruction of existing SWs by collision on the other side. MH causing moderate dynamic instability without shortening of WLs would favor the latter effect, whereas SH causing more extensive dynamic instability in association with significant shortening of WLs would compromise the latter effect. Nevertheless, further experimental and simulation model studies will be required to substantiate this interpretation.

Most previous studies in humans and animals have shown that hypothermia is associated with increased susceptibility for ventricular arrhythmias and VF (18, 23), and this effect has been related to the slowing of conduction, a heterogeneous increase in ventricular repolarization and the dispersion of refractoriness (21). However, there is experimental evidence suggesting the antiarrhythmic therapeutic potential of hypothermia (7, 10). In pigs

tapraid4/zh4-ahea/zh4-ahea/zh400508/zh48209d08z | xppws | S=1 | 3/5/08 | 12:14 | MS: H-00986-2007 | Ini: 05/JTG/BEW

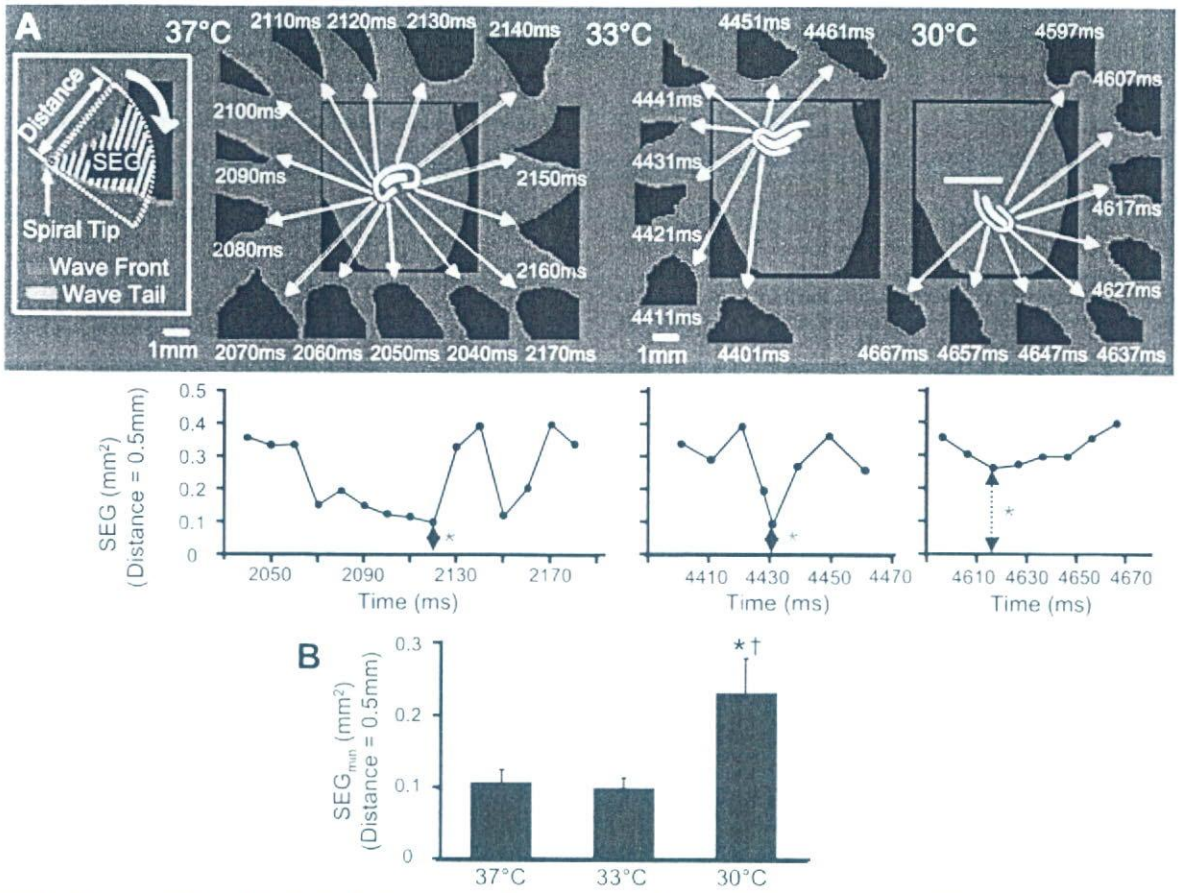

Fig. 8. Spatial excitable gap (SEG) of SW close to the rotation center. *A*: representative changes of SEG during rotation of SWs. SEG was estimated by measuring an area circumscribed by wave front (red), wave tail (green), and an arc with a certain distance (radius) from the spiral tip at 10-ms intervals. *A, top*: front-tail maps of SWs at NR (37°C), MH (33°C), and SH (30°C). SW selected for the analysis showed rotation >180° and were distant (>5 mm) away from any other SWs in the observation area. *A, bottom*: sequential changes of SEG at a distance of 0.5 mm (red asterisks indicate minimal values). *B*: average values of SEG at a distance of 0.5 mm from the spiral tip. Data were obtained from 5–9 SWs in each heart at the respective temperature (means ± SD, $n = 6$). *$P < 0.05$ vs. 37°C, †$P < 0.05$ vs. 33°C.

subjected to defibrillation shocks and cardiopulmonary resuscitation following unsupported VF, Boddicker et al. (3) showed that the defibrillation success and subsequent resuscitation outcome were improved by preexisting MH and SH, and the effect was most remarkable at MH. Some unidentified mechanical, metabolic, or electrophysiological properties were suggested to be involved in the beneficial effect of hypothermia in terms of prevention of refibrillation (3). In the present study, a certain modification of SW dynamics at MH could contribute to the in vivo prevention of refibrillation following DC shocks.

Limitations. First, we investigated the temperature-dependent alterations of DC stimulation-induced SW dynamics, and the results have revealed a destabilization and an early termination of SW excitations at MH. This observation may not directly translate to the mechanisms of defibrillation, where many other factors are involved (11). Second, the experiments were carried out using a 2-D subepicardial layer of rabbit ventricular myocardium. Extending these results to 3-D hearts, especially in larger animals including humans, is not straightforward. If there is sufficient tissue mass, the chance of spontaneous termination of rotors by mutual annihilation or collision with anatomical boundaries would be reduced, whereas the enhancement of wave breakup would increase the generation of new rotors in favor of VT/VF perpetuation. The greater structural discontinuities and functional heterogeneities in diseased hearts would also alter the spatial requirements of spontaneous rotor termination. Finally, we used BDM as an excitation-contraction uncoupler that is known to alter ionic currents, to reduce APD restitution slope and to affect intracellular Ca^{2+} dynamics (16). However, this does not seem to invalidate the present results, because the characteristic temperature-dependent modification of SW dynamics was preserved in the absence of BDM (see supplemental Fig. 3). Despite these limitations, the present study provides a new perspective for therapeutic potential of hypothermia in the treatment of serious recurrent VT/VF (electrical storm).

ACKNOWLEDGMENTS

We thank Prof. Jose Jalife (SUNY, Syracuse, NY) for critical reading of our manuscript. We also thank Dr. Kazuo Nakazawa (National Cardiovascular Center, Suita, Japan) for theoretical advice in completing the study.

GRANTS

This study was supported by the Health and Labor Science Research Grant for Research on Medical Devices for Analyzing, Supporting and Substituting